



OPEN ACCESS

EDITED BY

Ellen B. Stechel,
Arizona State University, United States

REVIEWED BY

Venkateshkumar Prabhakaran,
Pacific Northwest National Laboratory (DOE),
United States
Narayanamoorthy Bhuvanendran,
Dongguk University Seoul, Republic of Korea

*CORRESPONDENCE

Diogo M. F. Santos,
✉ diogosantos@tecnico.ulisboa.pt

RECEIVED 19 January 2024

ACCEPTED 14 March 2024

PUBLISHED 07 May 2024

CITATION

Araújo H, Šljukić B, Gago S and Santos DMF (2024), The current state of transition metal-based electrocatalysts (oxides, alloys, POMs, and MOFs) for oxygen reduction, oxygen evolution, and hydrogen evolution reactions. *Front. Energy Res.* 12:1373522. doi: 10.3389/fenrg.2024.1373522

COPYRIGHT

© 2024 Araújo, Šljukić, Gago and Santos. This is an open-access article distributed under the terms of the [Creative Commons Attribution License \(CC BY\)](https://creativecommons.org/licenses/by/4.0/). The use, distribution or reproduction in other forums is permitted, provided the original author(s) and the copyright owner(s) are credited and that the original publication in this journal is cited, in accordance with accepted academic practice. No use, distribution or reproduction is permitted which does not comply with these terms.

The current state of transition metal-based electrocatalysts (oxides, alloys, POMs, and MOFs) for oxygen reduction, oxygen evolution, and hydrogen evolution reactions

Henrique Araújo^{1,2}, Biljana Šljukić¹, Sandra Gago² and Diogo M. F. Santos^{1*}

¹Center of Physics and Engineering of Advanced Materials, Laboratory for Physics of Materials and Emerging Technologies, Chemical Engineering Department, Instituto Superior Técnico, Universidade de Lisboa, Lisbon, Portugal, ²Associated Laboratory for Green Chemistry (LAQV) of the Network of Chemistry and Technology (REQUIMTE), Department of Chemistry, NOVA School of Science and Technology (FCT NOVA), Campus da Caparica, Caparica, Portugal

Climate change is showing its impacts now more than ever. The intense use of fossil fuels and the resulting CO₂ emissions are mainly to blame, accentuating the need to develop further the available energy conversion and storage technologies, which are regarded as effective solutions to maximize the use of intermittent renewable energy sources and reduce global CO₂ emissions. This work comprehensively overviews the most recent progress and trends in the use of transition metal-based electrocatalysts for three crucial reactions in electrochemical energy conversion and storage, namely, the oxygen evolution (OER), oxygen reduction (ORR), and hydrogen evolution (HER) reactions. By analyzing the state-of-the-art polyoxometalates (POMs) and metal-organic frameworks (MOFs), the performance of these two promising types of materials for OER, ORR, and HER is compared to that of more traditional transition metal oxides and alloy-based electrocatalysts. Both catalytic activity and stability are highly influenced by the adsorption energies of the intermediate species formed in each reaction, which are very sensitive to changes in the microstructure and chemical microenvironment. POMs and MOFs allow these aspects to be easily modified to fine-tune the catalytic performances. Therefore, their chemical tunability and versatility make it possible to tailor such properties to obtain higher electrocatalytic activities, or even to obtain derived materials with more compelling properties towards these reactions.

KEYWORDS

hydrogen evolution reaction, oxygen evolution reaction, oxygen reduction reaction, electrocatalysts, polyoxometalates, metal-organic frameworks

1 Introduction

The world is facing an environmental crisis due to the overuse of carbon-emitting energy sources, namely, fossil fuels, for transportation or energy generation to power industry and domestic households, for example. This increases global greenhouse gas emissions, namely, CO₂, consequently increasing the global temperature.

This fact comes with devastating consequences, such as more intense and extreme weather events (droughts, heat waves, flooding, and heavy rainfall), and it also brings about a rise in sea levels (IPCC, 2018). As such, it was identified that it is necessary to effectively reduce carbon dioxide emissions to a net-zero level to limit the temperature increase to 1.5 °C as envisioned by the Paris Agreement signed by the United Nations (UN) members. Regarding the current global energy matrix, fossil fuels are a major contributor in many countries. They play a key role in supplying the energy necessary for proper economic and technological operations, accounting for over 80% of global energy consumption (Amin et al., 2022; Ritchie et al., 2022). However, the reduction in greenhouse gas emissions is mainly dependent on substituting fossil fuels (which are responsible for around 75% of these emissions) for cleaner and renewable energy sources, such as wind, solar, and hydropower energy, presenting themselves as powerful tools to combat the current climate crisis and to pave the way for a greener future.

Unfortunately, these renewable energy sources, especially wind and solar energy, which are the most abundant, have a highly intermittent character, meaning that there are periods where energy production peaks and periods where it declines (Amin et al., 2022; Chatenet et al., 2022). One solution to this intermittent character of renewable energy sources comes in the form of energy storage methods, generally via the use of batteries, which can store the surplus of electric energy during periods of low electricity demand and later release it during periods of high demand. This excess renewable energy can also be stored as green hydrogen (H₂) produced via water electrolysis, a concept known as Power-to-X. The produced green H₂ can be used for a panoply of applications, directly replacing typical grey H₂ produced from steam-methane reforming, or even act as an energy carrier for electricity generation in fuel cells during periods when energy production does not meet the total energy demand.

Thus, H₂ is seen as a promising energy carrier due to its high energy density, around 33 kWh/kg. Furthermore, the combustion of H₂ merely releases water vapor and energy, a crucial factor when considering its use as a green energy source. Specifically, green H₂ production is based on the electrochemical splitting of water powered by renewable energy sources. This process generates H₂ gas in the cathode through the hydrogen evolution reaction (HER) and oxygen (O₂) gas in the anode through the oxygen evolution reaction (OER), with no greenhouse gases emitted during the whole production process (Amin et al., 2022; Arcos and Santos, 2023). For this reason, green H₂ production and its use are widely considered a natural solution to end the energy and climate crisis, establishing the so-called hydrogen economy.

From the perspective of batteries and fuel cells, even though they have already been shown to work safely and effectively, there is an increasing need for the development of bifunctional materials that can be utilized to make them rechargeable and reversible. This

becomes relevant due to the need to reduce waste generation from the production and use of disposable batteries (Arcos and Santos, 2023). The relevant chemical reactions for rechargeable batteries and regenerative fuel cells are the oxygen reduction reaction (ORR) and the OER, which happen during the discharging and charging processes, respectively. Still on the topic of bifunctionality, materials with activity towards both the HER and the OER are also highly desired for alkaline water electrolysis technologies, mainly due to stability concerns.

However, the three aforementioned electrochemical reactions exhibit sluggish reaction kinetics (particularly the OER and ORR), meaning efficient electrocatalysts are needed to accelerate production. The best-performing ones are carbon-supported platinum (Pt/C) for HER and ORR, and iridium and ruthenium oxides (IrO₂ and RuO₂) for OER. These benchmark catalysts are expensive since they are based on scarce and precious metals, which increases total production costs. Much scientific effort is devoted to finding efficient, inexpensive, and stable electrocatalysts for the cited reactions, based mostly on common transition metals such as Ni, Co, Mn, and Cu.

Many strategies have been followed to produce effective electrocatalysts. Carbon supports have been widely applied, mainly due to the enhancement in electric conductivity and surface area, directly impacting performance. Examples of commonly tested supports are multi-walled carbon nanotubes (MWCNTs), single-walled carbon nanotubes (SWCNTs), reduced graphene oxide (rGO), graphene flakes (GFs), and carbon fiber paper (CFP) (Fernandes et al., 2018a; Liu et al., 2019; Jawale et al., 2022; Marques et al., 2022; Rehman et al., 2022). On the topic of organic supports, an exciting aspect to be aware of is the capability of including heteroatoms, such as N, in the final catalyst structure; this generally means carrying out an N-doping process on the support (Sun et al., 2015; Zhu et al., 2018; Wang C. et al., 2019; Jeong et al., 2020; Peng et al., 2020). Although N is the most popular dopant, other heteroatoms, such as F, S, P, and metals, are also applied (Zhang S. et al., 2017; Abdelkader-Fernández et al., 2019; Bhuvanendran et al., 2021).

Another method used to impact electrocatalytic activity is by modifying the catalyst composition. This can be done by adding other metals, mainly via alloying. An example is the reduction of Pt content in Pt-based electrocatalysts by alloying it with Ni or Fe (Vij et al., 2017; Zhang C. et al., 2017). This modifies the catalyst's electronic structure, combining the advantages of the alloyed metals, and enhancing the overall activity. The modifications in composition may also impact the catalysts' morphology. The production of octahedral (111) alloy PtNi nanoparticles, more effective for ORR than their cubic (100) Pt counterpart, has been shown to be dependent on composition when a solid-state chemistry method is utilized (Zhang et al., 2014). Still, on the topic of morphology-dependent activity, NiFe alloys are yet another example of how morphology can impact activity; alloys of those metals with hexagonal close-packed and face-centered cubic structures present quite different OER activities. Different morphologies have different surface areas, influencing the amount and type of exposed active sites and thus affecting catalytic activity.

Traditionally, oxide and alloy-based electrocatalysts are produced and tested, but new material classes, such as metal-organic frameworks (MOFs) and polyoxometalates (POMs) have been gaining interest recently due to their inherent advantages, mainly higher surface area due to their porous structures and their ability to be tailored for each

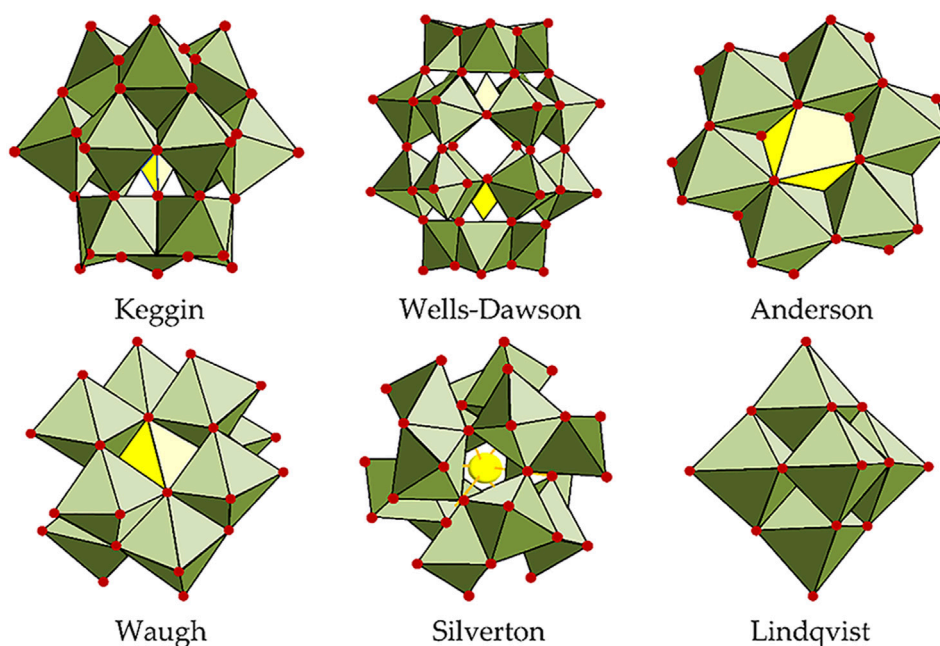


FIGURE 1 Polyoxometalates (POM) structures in polyhedral representations (Gusmão et al., 2022).

specific application due to the ease in modifying their structures (Jiang et al., 2016; Luo W. et al., 2017; Lu et al., 2017; Horn et al., 2021; Gusmão et al., 2022; Jia et al., 2022; Tseng et al., 2022). Briefly, MOFs are known to have a high abundance of metal active sites and can also act as templates to form other electrocatalysts. POMs have a high abundance of redox sites that can act as both acidic and basic sites and possess high thermal stability. Structurally, MOFs are formed by the linkage of inorganic metal ions/clusters and organic ligands, generating a 3D structure with long-range crystallinity, and POMs are metal (e.g., V, W, and Mo) oxide ion clusters linked together by oxygen atoms with a high number of redox centers.

This review summarizes the recent progress of transition metal-based POM (classic POM structures shown in Figure 1) and MOF electrocatalysts for the OER, ORR, and HER. It compares their advantages over the more traditional transition metal-based oxide and alloy electrocatalysts, which mainly reside in their higher chemical tunability and versatility, as shown in Figure 2 for MOFs. This allows, for example, tailoring properties, such as adsorption energy, to obtain higher electrocatalytic activity. For each relevant reaction, a series of electrocatalysts belonging to a different material class are analyzed, with advantages and disadvantages being highlighted regarding the class as a whole. General innovations brought by each reviewed work include the use of carbon and non-carbon materials as POM or MOF electrocatalyst supports, modifications in POMs' and MOFs' morphology stemming from varying the synthesis method and applying different precursors (leading to the production of bimetallic or even polymetallic electrocatalysts), and the introduction of dopants in the final catalyst structure, directly impacting their composition and providing different synergistic effects between the utilized elements, thus improving the catalytic activity as a whole.

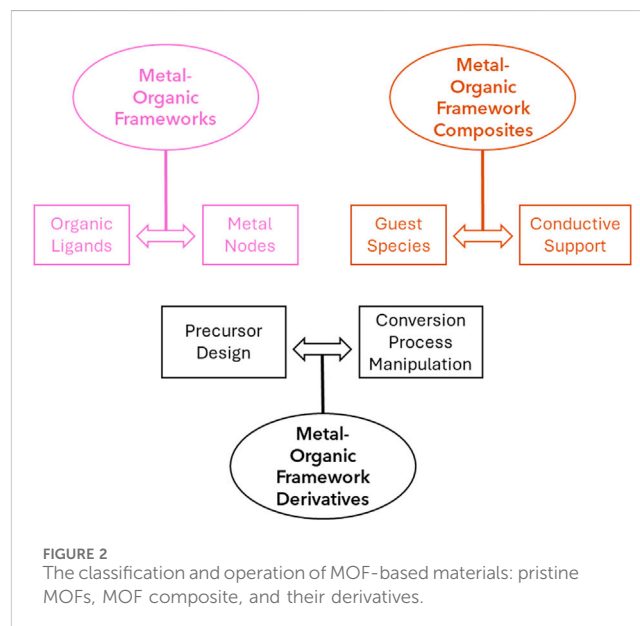


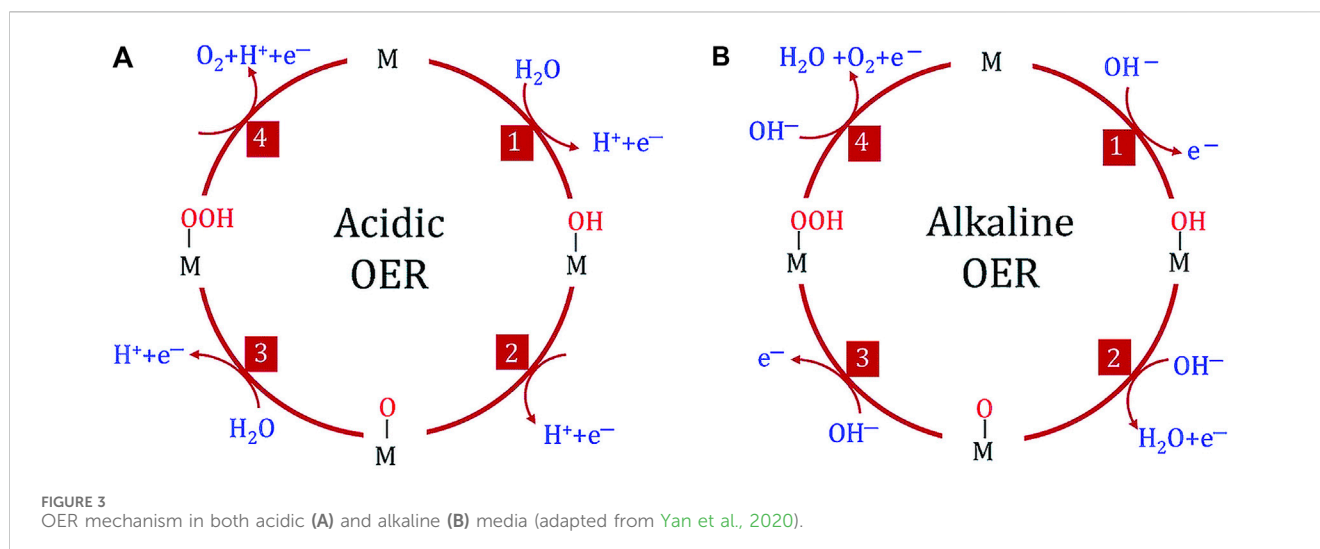
FIGURE 2 The classification and operation of MOF-based materials: pristine MOFs, MOF composite, and their derivatives.

2 Oxygen evolution reaction (OER)

The OER is an anodic reaction that can be carried out in alkaline (Equation 2.1) and acidic (Equation 2.2) media, releasing O_2 gas.



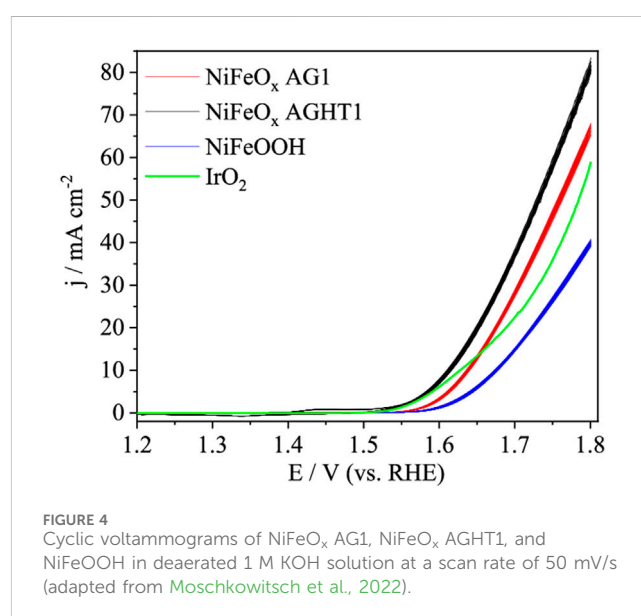
The equilibrium potential at standard conditions is ca. 1.23 V against the reversible hydrogen electrode (RHE). Still, to perform



this reaction at reasonable rates requires applying higher overpotentials (η) than those needed for the hydrogen evolution reaction (HER). This happens due to the sluggish kinetics of the OER caused by its inherent reaction mechanism that involves 4 proton-coupled electron transfer steps, as seen in Figure 3, resulting in higher activation energy (Xu et al., 2019; Chatenet et al., 2022; Gusmão et al., 2022). The reaction kinetics also differ depending on the pH: the OER presents more sluggish kinetics in acidic media when compared to alkaline media, which in turn causes the overpotential to achieve the same reaction rate to be higher in acidic media than in alkaline media (Tahir et al., 2017; Chatenet et al., 2022).

The need for a higher overpotential for the OER is also a bottleneck for alkaline water electrolysis, metal-air batteries (MAB), and regenerative fuel cells (RFC) since it is a main component of those technologies, and thus the high overpotentials contribute to higher energy consumption (Tahir et al., 2017; Chatenet et al., 2022). To reduce the high overpotentials associated with this reaction, electrocatalysts are applied to lower activation energies, increasing the reaction kinetics.

The most effective OER electrocatalysts to date are the noble-metal-based Ru and Ir oxides due to their remarkable activity, low overpotential, and excellent dissolution resistance in acidic conditions (Nakagawa et al., 2009; Jiang et al., 2018; Chatenet et al., 2022). This does not discard their use in alkaline conditions since they show good stability at all pH values (Katsunaros et al., 2014; Tahir et al., 2017). However, their main problem resides in their noble nature, meaning they are scarce metals with a high price, compromising their applicability on an industrial scale (Katsunaros et al., 2014; Tahir et al., 2017; Chatenet et al., 2022; Gusmão et al., 2022; Zeb et al., 2023). Because of these limitations, extensive efforts have been made to find cheaper alternatives to these noble-metal catalysts, mainly by utilizing more abundant transition metals such as Ni, Co, Cu, and Mn. These metals are more affordable, which facilitates their use in industrial conditions. Still, one should also be aware of the stability of these transition-metal-based electrocatalysts, which, in acidic conditions, is generally low (Goberna-Ferrón et al., 2015; Sun et al., 2015; Lu et al., 2019; Zand et al., 2023), hence why there are fewer studies on this type of media.



2.1 Transition metal oxides for OER

Metal oxides are commonly used electrocatalysts for OER due to their compositional and structural diversity, flexible tunability, low cost, abundance, and environmental friendliness (Mladenović et al., 2023a). Although pristine metal oxides are generally unsatisfactory for practical applications due to stability issues and unfavorable binding strength, mixed metal oxides are seen as a possible workaround due to the synergy of the properties of their pristine counterparts (Xu et al., 2022; Mladenović et al., 2023a; Pratama et al., 2023).

Moschkowitsch et al. studied Ni_xFe_yO_z aerogels with different Ni/Fe ratios for OER activity in 1 M KOH. The best-performing material, NiFeO_x AGHT1, surpassed the activity of the benchmark IrO₂ electrocatalyst (Figure 4). The Ni/Fe ratio greatly affected the catalytic performance, and the best-performing sample had 6 at% Fe, surpassing the NiO_x aerogel and showing that Fe has synergistic effects in the nickel oxide

structure and that aerogels, which were initially only thought to act as supports, could also act as electrocatalysts (Moschkowitsch et al., 2022).

A phosphorus-modified hollow porous nickel-cobalt oxides nanocube with varying P content was tested for OER in 1 M KOH. The optimum P-NiO/NiCo₂O₄ sample was stable and presented an overpotential of 290 mV for a current density of 10 mA/cm² and a Tafel slope of 49.6 mV/dec, outperforming even the benchmark RuO₂ electrocatalyst. The superior performance was attributed to the effect of P-doping, which decreased the energy barrier, optimized the adsorption of intermediates, and changed the rate-determining step, and to the hollow porous hybrid structure and oxygen vacancies that increased the amount of exposed surface area (Zhang L. et al., 2022).

Similarly, Luo X.-F et al. tested, in alkaline medium (1 M KOH), MnO_x oxides grown directly on Ti foil via electrodeposition with different morphologies obtained at different reaction temperatures: cotton wool structure, nanowire arrays, and nanosheet arrays. The nanowire arrays proved to be the best-performing material in the study, presenting an OER onset potential of 1.546 V vs RHE, a Tafel slope of 106 mV/dec, and a current density of 44.7 mA/cm² when an overpotential of 538 mV is applied. The performance of the nanowire arrays was attributed to a larger surface area due to the direct growth of the nanostructure on the Ti foil support, which enhanced conductivity (Luo et al., 2017b). Alternatively, Zand et al. tested MnO_x and silicate-stabilized MnO_x in acidic medium (0.1 M H₂SO₄) and demonstrated that the poor stability of the Mn oxide in acidic conditions can be significantly improved by adding silicate to the structure of the Mn oxide. The results showed that the catalytic activity was less than optimal since the overpotential needed to achieve 10 mA/cm² was 640 mV, and the OER onset potential was 1.757 V vs RHE. On the other hand, the stability was greatly improved because the modified Mn oxide showed higher current retention and virtually no structural changes after OER (Zand et al., 2023).

Zhang et al. evaluated copper-doped cobalt oxides deposited via a reactive DC magnetron sputtering process as electrocatalysts for OER in alkaline medium (1 M KOH). The mixed oxides demonstrated relevant activity and showed that copper doping improved the electrocatalytic performance with respect to the single metal cobalt and copper oxides. The best-performing mixed oxide, Cu_{1.97}CoO₃, demonstrated a performance close to that of RuO₂. The increase in activity was attributed to changes in crystal structure and morphology that increased the surface-active area (Zhang et al., 2012). Later, Park et al. tested a nanosized synthetic Cu_{0.7}Co_{2.3}O₃ oxide prepared using a thermal decomposition method in alkaline medium (1 M KOH) for OER. The overpotential necessary to obtain a 10 mA/cm² current density was around 491 mV (Park et al., 2016). Xu et al. studied a cerium-doped cobalt oxide (CoO_x(Ce)) in the form of an amorphous film deposited through an electrostatic spray deposition method. It presented an OER onset potential of 1.315 V vs RHE, an overpotential of 261 mV to achieve a 20 mA/cm² current density, and a Tafel slope of 65.7 mV/dec for OER in 1 M KOH, exhibiting higher performance than regular CoO_x, other cerium doped OER catalysts and even commercially available RuO₂. The better performance was attributed to the increase in the electrochemical active surface area (ECSA) caused by the resulting sample's

amorphous nature and the formation of cerium-related oxygen vacancies without modifying the cobalt species (Xu et al., 2019).

Roy et al. tested a self-supported copper oxide electrocatalyst grown on Ni foam substrate via an electrodeposition method, demonstrating suitable activity for OER in a 1 M KOH solution. The best-performing material, CuO/Ni@400, presented an overpotential of 364 mV and 508 mV to achieve a 10 mA/cm² and a 100 mV/cm² current density and a Tafel slope of 90 mV/dec, while also presenting stability in alkaline medium by maintaining constant current density. The superior performance of CuO/Ni@400 was attributed to its microstructure, which made an even way for electron tunneling (Roy et al., 2019). Likewise, Wang et al. tested an in situ-produced copper foam-supported copper oxide (CuO-A/CF) sample prepared via the oxidation of copper selenide (Cu₂Se) at OER conditions in 1 M KOH. The as-prepared electrocatalyst presented an overpotential of 297 mV to achieve a current density of 10 mA/cm² and a Tafel slope of 72.8 mV/dec, pointing to fast electron and mass transfer between the catalyst and the electrolyte. The superior performance relative to CuO produced from calcination of Cu(OH)₂ supported in copper foam is attributed to the nanoplate structure of CuO-A/CF, which increased the available electrochemical surface area. The catalyst stability was also stated by testing over 50 h in 1 M KOH at a constant 10 mA/cm² current density, maintaining a constant overpotential over this period and showing no structural changes (Wang et al., 2020).

Ye et al. tested various iron-copper oxides with different Cu/Fe ratios for OER in 1 M KOH. The oxide that demonstrated the best performance was 6CuO₂-Fe₂O₃, with an overpotential of 510 mV for 10 mA/cm². All the samples were stable in the reaction conditions. The performance was attributed to the coexistence of the metal oxides, but the overpotentials are still high, which shows that further improvements can be made (Ye et al., 2022). Similarly, Bai L. et al. tested amorphous ternary Fe-Co-Ni oxides, FeNiCoO_x, in alkaline medium (1 M KOH). The tests were made by depositing the material on a glassy carbon electrode and on a Ni foam electrode, which resulted in overpotentials of 240 and 203 mV and Tafel slopes of 45 and 75 mV/dec, respectively, showing a much better performance than the mono or binary metal oxides of those elements and showcasing good stability properties. This increase in catalytic performance was attributed to the synergistic interactions between the three employed metals in the oxide, which greatly reduced the charge transfer resistance and their homogeneous distribution in the oxide (Bai L. et al., 2019).

The OER performance parameters of the above-cited transition metal oxide-based catalysts are shown in Table 1. However, due to the generally high overpotentials presented by the metal oxides (Park et al., 2016; Xing et al., 2018; Sivakumar et al., 2019; Ye et al., 2022; Zand et al., 2023) and their generic instability in acidic medium (Zand et al., 2023), scientists have also tested another traditional catalyst class: transition metal alloys.

2.2 Transition metal alloys for OER

Alloy compounds are sought out due to their low cost and high OER/HER catalytic activity. Their high versatility by including different metals (forming binary, ternary, or multicomponent

TABLE 1 OER electrocatalysts and their key performance indicators: transition metal oxides.

Electrocatalyst	η_{10} (mV)	Tafel slope (mV/dec)	Electrolyte	Source
NiFeO _x AGHT-1	380	-	1 M KOH	Moschkowitsch et al. (2022)
P-NiO/NiCo ₂ O ₄	290	49.6	1 M KOH	Zhang et al. (2022b)
MnO _x nanowire arrays	538@44.7 mA/cm ²	106	1 M KOH	Luo et al. (2017b)
SiO ₄ /MnO ₂	640	-	0.1 M H ₂ SO ₄	Zand et al. (2023)
Cu _{1.97} CoO ₃	-	70.15	1 M KOH	Zhang et al. (2012)
Cu _{0.7} Co _{2.3} O ₃	491	-	1 M KOH	Park et al. (2016)
CoO _x (Ce)	261@20 mA/cm ²	65.7	1 M KOH	Xu et al. (2019)
CuO/Ni@400	364	90	1 M KOH	Roy et al. (2019)
CuO-A/CF	297	72.8	1 M KOH	Wang et al. (2020)
6CuO ₂ -Fe ₂ O ₃	510	-	1 M KOH	Ye et al. (2022)
FeNiCoO _x /GC	240	45	1 M KOH	Bai L. et al. (2019)
FeNiCoO _x /NF	203	75	1 M KOH	Bai L. et al. (2019)

alloys) also allows for selectivity and activity enhancement in the final alloy. Another advantage of alloying is that Pt-based materials can be synthesized with similar or higher catalytic activity while lowering Pt content, which inevitably lowers production costs on a large-scale perspective (Mladenović et al., 2021; Mladenović et al., 2022; Mladenović et al., 2023b; Xu et al., 2023).

Lim et al. reported the synthesis of bimetallic NiFe alloy nanoparticles used as electrocatalysts for the OER in alkaline medium (1 M KOH). The produced alloy presented much better activity than its unary metal Ni and Fe counterparts, having an overpotential of 298 mV for 10 mA/cm² and a Tafel slope of 51.9 mV/dec, surpassing the performance of state-of-the-art RuO₂ electrocatalyst. This performance was attributed to the synergistic effects between the metals and the modification of redox properties of Ni sites and the electronic structure of Ni atoms due to the presence of the Fe atoms, as well as the partial oxidation of the alloy into metal oxyhydroxides (Lim et al., 2020). Wang C. et al. reported the synthesis of a hexagonal close-packed (hcp) crystal structure in NiFe alloys and its use as an OER catalyst in alkaline medium (1 M KOH). The samples of different Fe/Ni ratios were supported on N-doped carbon shell structures. The electrocatalytic performance of the best sample (with Fe/Ni ratio of ca. 5.4 at.%) surpassed that of regular face-centered cubic (fcc) NiFe and commercially available RuO₂, needing an overpotential of 226 mV to achieve 10 mA/cm² and a Tafel slope of 41 mV/dec, and showed promising stability properties. The performance was attributed to the interaction between the intrinsic crystal structure and the carbon shell, resulting in different electronic properties at its surface that favored the OER process (Wang C. et al., 2019).

From another perspective, Jeong et al. determined the effects of using graphene-encapsulated porous NiMo alloys and compared them to bare porous NiMo alloys for OER in an alkaline medium (1 M KOH). The results showed that the graphene encapsulation enhanced the catalytic performance of the alloy by lowering the overpotential necessary to achieve 10 mA/cm² and the Tafel slope from 396 to 351 mV and 101 to 69 mV/dec, respectively, resulting in a performance similar to RuO₂. The stability in 1 M KOH also

increased when supported in nickel foam by impeding the degradation of the metals into oxides and hydroxides. The better performance was assigned to synergistic effects between N-doped graphene and NiMo alloy that impacted the adsorption of intermediates, optimizing the free adsorption energies and accelerating the OER rate-determining step (Jeong et al., 2020).

Dai et al. studied a MnFeCoNi high entropy alloy activated for OER through a cyclic voltammetry treatment in an alkaline medium (1 M KOH). The activated alloy exhibited an overpotential of 285 mV to reach a 10 mA/cm² current density, presented a Tafel slope of 83.7 mV/dec, and showed good stability properties, surpassing the benchmark RuO₂ catalyst. The catalytic activation of the high entropy alloy was attributed to the formation of monometallic oxides of the metals dispersed as nanosheets throughout the particle's surface, which acted as the true catalyst for OER and exposed more active sites (Dai et al., 2019).

Li et al. tested the use of 3D hierarchical flower-like materials composed of ultrathin cobalt-based bimetallic phosphide nanosheets (CoM-P-3DHFLMs, M = Mn, Cu, Ni) in a 1 M KOH solution for OER catalysis. The CoNi-P-3DHFLM, CoMn-P-3DHFLM, and CoCu-P-3DHFLM samples presented an overpotential of 292, 318, and 307 mV to reach 10 mA/cm² and Tafel slopes of 84, 98, and 88 mV/dec, respectively, along with good stability. The enhanced performance compared to Co-P-3DHFLM was attributed to a synergistic interaction between the metals and to the exposition of more active sites in the bimetallic samples (Li et al., 2019).

Bai X. et al. used Co-Fe-based spherical nanoparticles coated with an amorphous carbon shell, whose active species was a Co₇Fe₃ alloy, for OER in alkaline medium (1 M KOH). This material showed an overpotential of 272 mV for 10 mA/cm² and a Tafel slope of 40 mV/dec, surpassing most of their monometallic-based counterparts while remaining stable under the reaction conditions. The performance was attributed to the synergy between Co and Fe due to their strong electronic interaction, which lowered the activation energy for OER, favoring the reaction kinetics (Bai X. et al., 2021). Liu et al. presented the synthesis of a P-modified hollow, highly porous, and conductive CoFe alloy (Fe-Co-P) nanosphere

TABLE 2 OER electrocatalysts and their key performance indicators: transition metal alloys.

Electrocatalyst	η_{10} (mV)	Tafel slope (mV/dec)	Electrolyte	Source
NiFe NPs	298	51.9	1M KOH	Lim et al. (2020)
Hep-phase NiFe NPs	226	41	1 M KOH	Wang C. et al. (2019)
NiMo-FG	351	69	1 M KOH	Jeong et al. (2020)
MnFeCoNi	285	83.7	1 M KOH	Dai et al. (2019)
CoNi-P-3DHFLM	292	84	1 M KOH	Li et al. (2019)
CoMn-P-3DHFLM	318	98	1 M KOH	Li et al. (2019)
CoCu-P-3DHFLM	307	88	1 M KOH	Li et al. (2019)
Fe ₁ Co ₃ O _x @C-800	272	40	1 M KOH	Bai X. et al. (2021)
Fe-Co-P	252	33	1 M KOH	Liu et al. (2018)
Co _{0.5} Ni _{0.5} /rGO	288	103	1 M KOH	Zhang et al. (2020)
Cu _{3.8} Ni@C	233	114	1 M KOH	Kumar et al. (2020)
Cu-N-C NA/CF	314@20 mA/cm ²	115	1 M KOH	Zhu et al. (2018)
FeCoCu	265	49	1 M KOH	Jiang et al. (2021)
FeCoCuNi	269	48.9	1 M KOH	Jiang et al. (2021)

structure and tested it for OER in alkaline medium (1 M KOH). It was determined that the optimized alloy for OER had a 3:2 Fe/Co ratio and showed an overpotential of 252 mV to reach 10 mA/cm² and a Tafel slope of 33 mV/dec, while also presenting very good stability in the reaction conditions. The enhanced performance of the electrocatalyst was attributed to the high valent state of Fe stabilizing the low valent state of Co and the alloy formation being able to fine tune the energetics of all the intermediates involved in the water oxidation mechanism (Liu et al., 2018).

Zhang et al. reported the application of a coral-like carbon-wrapped NiCo alloy (Co_{0.5}Ni_{0.5}/rGO) for OER at alkaline conditions (1 M KOH). The sample showed an overpotential of 288 mV to achieve 10 mA/cm² and a Tafel slope of 103 mV/dec, while demonstrating stability in the tested conditions, surpassing their monometallic counterparts and the benchmark RuO₂ catalyst in the same conditions. The improved performance is attributed to the graphene sheets introducing a more homogeneous metal distribution, thus exposing more active sites, and to the synergistic interaction between Ni and Co, with Ni regulating the electronic structure of Co, favoring the OER performance (Zhang et al., 2020).

Kumar et al. described the use of bimetallic copper-nickel alloy nanorods textured nanoparticles supported on graphitic carbon (Cu_{3.8}Ni@C) samples for OER in alkaline conditions (1 M KOH). The best-performing sample presented an overpotential of 233 mV for 10 mA/cm² and a 114 mV/dec Tafel slope and good stability properties, which fared well against state-of-the-art IrO₂ (Kumar et al., 2020). Zhu et al. disclosed the use of a Cu nanoparticles-embedded N-doped carbon nanowire array on copper foam (Cu-N-C NA/CF) as an OER electrocatalyst in alkaline medium (1 M KOH). The sample presented an overpotential of 314 mV to reach 20 mA/cm², a Tafel slope of 115 mV/dec, and was demonstrated to be a stable catalyst in OER conditions for at least 16 h. The performance was attributed to the *in-situ* formation of CuO nanoparticles, which acted as the true OER catalyst, and to the increased electrochemical surface area, which exposed

more active sites (Zhu et al., 2018). Jiang et al. tested a series of Cu-based alloys (CuM, M = Fe, Co, Ni; FeCo, FeNi, CoNi; FeCoNi) for OER in an alkaline electrolyte (1M KOH). The FeCoCu and FeCoNiCu samples presented, after optimization, an overpotential of 265 and 269 mV for 10 mA/cm² and Tafel slopes of 49 and 48.9 mV/dec, respectively, along with proper stability properties, outperforming the benchmark RuO₂ electrocatalyst. The enhanced performance relative to Cu was attributed to synergistic effects between the highly conductive Cu and the OER active Fe, Co, and Ni elements (Jiang et al., 2021).

Table 2 presents the performance parameters for each analyzed OER alloy-based catalyst. Metals and alloys often cannot survive in harsh acidic or basic environments mainly due to the strongly corrosive media, meaning they have to frequently be embedded or decorated in relatively stable hosts, such as carbon materials (Wu et al., 2020). This, amongst other reasons, fueled researchers to investigate more compelling and innovative materials, such as MOFs.

2.3 Transition MOFs and MOF-derived electrocatalysts for OER

MOFs are a class of porous organic-inorganic hybrid materials formed by the linkage of inorganic metal ions/clusters and organic ligands, generating a 3D structure with long-range crystallinity. Recently, MOFs have gained attention from scientists due to their inherent properties, including high surface area, low density, high porosity, and tunable structure. Additionally, they are known for their abundance of metal active sites, utility as templates to generate other materials, and the high adjustability of chemical components (Jiang et al., 2016; Lu et al., 2017; Jia et al., 2022; Tseng et al., 2022). MOFs have found numerous applications, such as in catalysis, gas storage and separation, optics, drug delivery, adsorption, and chemical sensing (Lu et al., 2017; Li et al., 2020; Jia

et al., 2022). As such, research efforts have also been dedicated to producing cost-effective and high-performance electrocatalysts based on pristine MOFs or MOF-derived materials for applications in the OER, HER, and ORR.

Ma et al. reported the *in-situ* synthesis of MOF-encapsulated bimetallic nanoparticles by etching Ni-Cu alloy nanoparticles without additional metal precursors and its performance for alkaline OER (1 M KOH). The bimetallic encapsulated MOF had better activity than its monometallic counterparts, showing a current density 1.6 and 71 times higher than for the Ni encapsulated and Cu encapsulated MOFs, respectively, at an overpotential of 624 mV and a Tafel slope of 98 mV/dec, and good stability. The higher activity was attributed to a higher number of exposed active sites and to synergistic effects between the Ni and Cu metals (Ma et al., 2019).

Tseng et al. disclosed the use of NiFe bimetallic MOFs deposited on pretreated nickel foam (NF) and processed by low-pressure plasmas with different composition atmospheres as OER electrocatalysts in alkaline electrolyte (1 M KOH). The electrocatalytically optimized sample, NiFe-MOFs/NF-AH, treated with a 95% argon +5% H₂ atmosphere, presented an overpotential of 149 mV to achieve 10 mA/cm² and a Tafel slope of 54 mV/dec, along with good stability (Tseng et al., 2022). MOFs are often used as precursors for low-cost highly-active electrocatalysts. One example comes from Jiang et al., who used Fe-Ni-based MOFs as self-templates to synthesize several Fe-Ni-O_x oxide architectures with different Fe/Ni ratios and tested those for OER in alkaline medium (0.1 M KOH). The obtained results indicated that the performance was closely related to the Fe/Ni ratio, and the optimized sample, Fe_{0.5}Ni_{0.5}O_x, needed a 584 mV overpotential to achieve 10 mA/cm² and had a Tafel slope of 72 mV/dec, with good stability properties and performance comparable to that of benchmark RuO₂ catalyst. The performance is attributed to the *in-situ* formation of NiOOH and to the presence of spinel NiFe₂O₄ species, which act as the active phases for OER (Jiang et al., 2016).

Ji et al. detailed the synthesis of a marigold flower-like MOF-aided manganese vanadium oxide and its OER performance in alkaline medium (1 M KOH). The MOF MnV oxide microflower required a 310 mV overpotential to reach 50 mA/cm² and had a Tafel slope of 51.4 mV/dec, comparing its performance to the benchmark RuO₂ electrocatalyst and outperforming the monometallic MOF Mn and MOF V oxide microflower counterparts while also being able to sustain OER for over 50 h at a current density of 50 mA/cm². The activity was attributed to a higher number and exposition of active sites (Ji et al., 2023).

Zhao et al. assembled CoNi-based ultrathin MOF nanosheets (NiCo-UMOFNs) and tested them for OER in alkaline conditions (1 M KOH). The bimetallic MOF nanosheets presented an overpotential of 250 mV to reach 10 mA/cm², a Tafel slope of 42 mV/dec, and good stability properties, outperforming its monometallic counterparts and the benchmark RuO₂ electrocatalyst, especially when supported in copper foam, since the overpotential to reach 10 mA/cm² reduces to 189 mV. The performance was attributed to the existence of unsaturated metal sites and to the coupling effect between Ni and Co metals (Zhao et al., 2016). Zhou et al. designed a series of isostructural hierarchical bimetallic CoNi MOF nanostructures (CTGU-10a2-d2) with different Co/Ni ratios and tested them towards OER in an alkaline electrolyte (0.1 M KOH). The best performing MOF, CTGU-10c2, presented an overpotential of 240 mV to achieve 10 mA/cm², a Tafel slope of 58 mV/dec, and was stable in the OER conditions, surpassing the performance of the benchmark RuO₂ electrocatalyst. This performance was attributed to synergistic effects between the metal atoms, the hierarchical nanobelt structure, and the presence of unsaturated metal sites (Zhou et al., 2019).

Li et al. produced a Cu-based MOF directly supported on copper foam (MOF [Cu(OH)₂]/CF) and tested its activity towards OER in alkaline medium (1 M KOH). The resulting material used an overpotential of 330 mV to achieve 10 mA/cm² and had a Tafel slope of 108 mV/dec, with activity comparable to the RuO₂ electrocatalyst, while presenting good durability. The performance is attributed to the exposition of more active sites and to the *in-situ* formation of Cu oxide species, which act as active electrocatalysts towards OER (Li et al., 2020). Cheng et al. studied a bimetallic Cu-Co-based MOF nanobox as an OER electrocatalyst in alkaline medium (1 M KOH). The material required an overpotential of 271 mV to reach 10 mA/cm² and presented a Tafel slope of 63.5 mV/dec, all while being stable in the OER conditions, outperforming the monometallic counterparts and the benchmark RuO₂ electrocatalyst. The improved performance was attributed to the *in situ* formation of the bimetallic oxyhydroxide, which acts as the true catalyst with intrinsically higher electrocatalytic performance, synergistically enhanced by the Cu sites, while the Co sites act as the active ones (Cheng et al., 2021).

Table 3 presents a compilation of the analyzed MOFs OER performance parameters. In general, MOFs present poor electrical conductivity, poor stability, low mass permeability, and blockage of

TABLE 3 OER electrocatalysts and their key performance indicators: transition MOFs.

Electrocatalyst	η_{10} (mV)	Tafel slope (mV/dec)	Electrolyte	Source
Ni-Cu@Cu-Ni-MOF	-	98	1 M KOH	Ma et al. (2019)
NiFe-MOFs/NF-AH	149	54	1 M KOH	Tseng et al. (2022)
Fe _{0.5} Ni _{0.5} O _x	584	72	1 M KOH	Jiang et al. (2016)
MOF MnVO microflower	310@50 mA/cm ²	51.4	1 M KOH	Ji et al. (2023)
NiCo-UMOFNs	250	42	1 M KOH	Zhao et al. (2016)
CTGU-10c2	240	58	0.1 M KOH	Zhou et al. (2019)
MOF[Cu(OH) ₂]/CF	330	108	1 M KOH	Li et al. (2020)
CoCu-MOF-NBs	271	63.5	1 M KOH	Cheng et al. (2021)

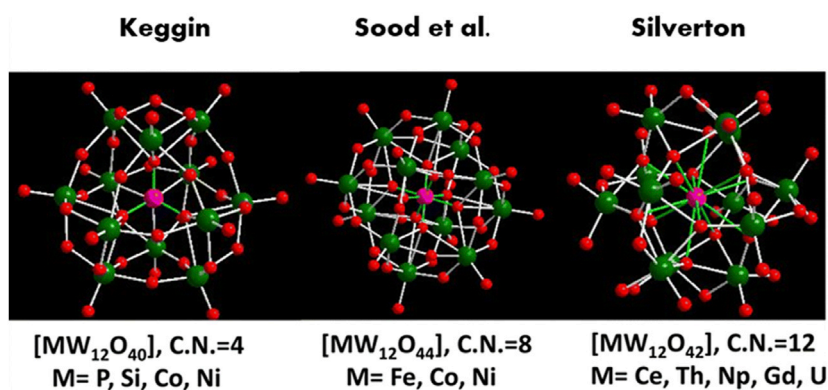


FIGURE 5
Different hetero-polyoxometalates belonging to the 1:12 series of POMs with various heteroatoms (adapted from Sood et al., 2022).

metal centers by organic ligands (Zhao et al., 2016; Lu et al., 2019; Ma et al., 2019), limiting their use in electrocatalytic applications. A way to circumvent this is the utilization of MOF-derived electrocatalysts, normally via calcination, to generate carbon materials with enhanced conductivity and stability. In spite of this, POMs have been studied as an alternative to MOF and MOF-derived electrocatalysts.

2.4 Transition metal POMs for OER

Amidst the collective effort to find alternatives to the noble metal-based electrocatalysts, POMs have appeared as a viable and highly sought-out alternative. POMs are inorganic redox-active transition metal (e.g., V, W, and Mo) oxide ion clusters linked together by oxygen atoms with a high number of redox centers, which grants them significant advantages when multi-step electron transfer reactions are involved (Horn et al., 2021; Gusmão et al., 2022). Other positive aspects of POMs include stability under oxidative OER conditions, thermal stability, rapid and highly reversible electrochemical activity, and finely tunable structures to suit the specific application needs (Luo W. et al., 2017; Horn et al., 2021; Gusmão et al., 2022).

They possess an ordered 3D framework structure that can be easily tailored to introduce redox-active transition metals (that can act as redox centers) into the framework. POMs can serve as structural agents to form nanostructures with other types of materials, such as oxides. Additionally, they can be encapsulated in various materials, such as MOFs, to derive the so-called POMOFs. These examples showcase the versatility that POMs offer (Horn et al., 2021). Still, one cannot overlook the conductivity and stability problems present in POMs, which can fortunately be circumvented by combining them with appropriate supports, such as carbon-based supports, organic supports, or by confining them in MOFs or Covalent Organic Frameworks. The incorporation of POMs in a more conductive support with adequate binding strength can prevent leaching problems and inhibit agglomerations, both increasing stability and maximizing the number of active sites present (Wang C. et al., 2023). Relative to the catalysis application, the Keggin variation structure is best suited due to

its proton binding sites and electron-rich oxygen sites, which participate in acid and base-catalyzed reactions, respectively. A variation of the Keggin structure is the lacunary Keggin structure, which results from removing a M=O moiety, and M can be substituted by a transition metal such as Ni, Mn, Co, or Cu to increase the redox catalytic properties (Horn et al., 2021; Gusmão et al., 2022).

Imani et al. produced a Keggin tungsten POM containing organic-inorganic hybrid composite material directly on a carbon paste electrode and later incorporated Ni and Fe ions (Ni-Fe/oA-POM/CPE). Afterward, they tested its performance towards OER in an alkaline electrolyte (0.1 M NaOH). The resulting composite required a 330 mV overpotential to reach 10 mA/cm² and had a Tafel slope of 113 mV/dec. It presented good stability in alkaline OER conditions, since after 10 h at a constant overpotential of 300 mV, it lost almost no activity, with a minor decrease after 500 cycles (Imani et al., 2018).

Sood et al. constructed a rare POM cluster-based solid, (C₅H₇N₂)₆[NiW₁₂O₄₄], whose structure is shown in the center section of Figure 5, and tested its performance towards OER in alkaline medium (1 M KOH). The synthesized POM was able to provide 10 mA/cm² at 347 mV of overpotential and showed a 130 mV/dec Tafel slope. It maintained a current density of 10 mA/cm² for up to 96 h, indicating good stability and outperforming state-of-the-art RuO₂ electrocatalyst. The observed performance was attributed to the *in situ* formation of WO_x (x = 1,2) and NiO, Ni(OH)₂, and NiOOH, which act as active phases in the electrocatalyst (Sood et al., 2022).

Al-Oweini et al. were the first ones to report the activity of a tetramanganese [Mn^{III}₃Mn^{IV}O₄(CH₃COOH)₃(A-αSiW₉O₃₄)₆]⁶⁻ POM towards photocatalytic OER in acid conditions (a pH 5 buffer was used) (Al-Oweini et al., 2014). Goberna-Ferrón et al. researched the electrocatalytic activity of a tetramanganese [Mn₄(H₂O)₂(PW₉O₃₄)₂]¹⁰⁻ sandwich-type POM towards OER in neutral conditions. The tested POM showed considerable activity for OER, although it reached negligible levels after 30 min. This was owed to the formation of MnO₂, which is inactive for water oxidation, indicating degradation and instability of the POM under harsh oxidative reaction conditions. The same effect was observed when the POM was used as a heterogeneous catalyst (Goberna-Ferrón et al., 2015).

Imani et al. designed a Mn-containing POM-based composite that was later deposited onto a rotating carbon paste electrode by two

TABLE 4 OER electrocatalysts and their key performance indicators: transition metal POMs.

Electrocatalyst	η_{10} (mV)	Tafel slope (mV/dec)	Electrolyte	Source
Ni-Fe/oA-POM/CPE	330	113	0.1 M NaOH	Imani et al. (2018)
(C ₅ H ₇ N ₂) ₆ [NiW ₁₂ O ₄₄]	347	130	1 M KOH	Sood et al. (2022)
Mn/oMA-PW/RCPE	380	111	1 M KOH	Imani et al. (2021)
Mn-oMA-PW + RCPE	440	133	1 M KOH	Imani et al. (2021)
FeCoPMo ₁₂	258	33	1 M KOH	Zhai et al. (2017)
CNCP-6	241	75.8	1 M KOH	Kang et al. (2022)
NiCo-POM/Ni	360	126	0.1 M KOH	Luo et al. (2017a)
SiW ₉ Co ₃ @ZIF-67	470	113.6	0.1 M KOH	Abdelkader-Fernández et al. (2020)
SiW ₉ Co ₃ @ZIF-8	-	69.4	0.1 M KOH	Abdelkader-Fernández et al. (2020)
[Cu ₃ (SbW ₉ O ₃₃) ₂ (H ₂ O) ₃] ¹²⁻	-	113	80 mM Tris-HCl solution	Yu et al. (2018)

immobilization methods: direct formation and physical mixing. The resulting electrodes were tested for OER in basic medium (1 M KOH), attaining a 380 and 440 mV overpotential to reach 10 mA/cm² and a Tafel slope of 111 and 133 mV/dec, respectively. In terms of stability and durability, they were able to perform for over 10 h while retaining 93.6% and 93.3% of current density, showing a small increase in overpotential (18 and 20 mV, respectively) after 600 cycles to keep 10 mA/cm² (Imani et al., 2021).

Zhai et al. disclosed the synthesis of FeCoPMo₁₂ POM through a room-temperature coprecipitation method, resulting in a porous and amorphous compound tested for OER in alkaline electrolyte (1 M KOH). The POM presented an overpotential of 258 mV to reach 10 mA/cm², a Tafel slope of 33 mV/dec, and stability for over 10 h of OER with a current loss of 8.3%, surpassing FePMo₁₂, CoPMo₁₂ and hydroxide counterparts, and benchmark RuO₂ electrocatalyst. The performance was attributed to the synergistic effects of Fe incorporation, which activates the active sites (Zhai et al., 2017).

Kang et al. reported the synthesis and use of dodecahedral Co, N, and C co-doped POMs with a frame-like yolk-shell nanostructure as OER electrocatalysts in an alkaline solution (1 M KOH). After optimization, the best-performing sample required an overpotential of 241 mV to achieve 10 mA/cm², while also having a Tafel slope of 75.8 mV/dec and long-term electrochemical stability (over 24 h with only a slight change in the output current density), outperforming the benchmark IrO₂ electrocatalyst. The performance is credited to uniform N, C, and Co doping and a higher exposition of active sites (Kang et al., 2022).

Luo W. et al. described the deposition of Dexter-Silverton POM microcrystals, Co_{6,8}Ni_{1,2}W₁₂O₄₂(OH)₄(H₂O)₈, in a nickel foam substrate and its use as an OER electrocatalyst in alkaline medium (0.1 M KOH). The resulting composite needed a 360 mV overpotential to reach a 10 mA/cm² current density and showed a Tafel slope of 126 mV/dec, while also retaining 85% of its current density in a 10 h test at a 440 mV overpotential test with no degradation of its crystal structure and morphology (Luo W. et al., 2017).

Abdelkader-Fernández et al. reported the synthesis of two POM@MOFs hybrids, SiW₉Co₃@ZIF-8 and SiW₉Co₃@ZIF-67, and tested their activities towards OER in 0.1 M KOH

electrolyte. It is demonstrated that the SiW₉Co₃@ZIF-67 hybrid has a more effective electron transfer process due to the presence of Co²⁺ nodes in the ZIF-67 skeleton, resulting from a synergistic interaction between the Co-based-POM encapsulated in the Co-based-MOF. This effect increases performance greatly: the resulting SiW₉Co₃@ZIF-67 presented a performance that well exceeded benchmark RuO₂ and IrO₂ electrocatalysts even though these benchmark materials exhibit higher “intrinsic” non-area dependent performances towards the OER in the roughness-corrected polarization curves (Abdelkader-Fernández et al., 2020).

Yu et al. studied the activity of the sandwich-type [Cu₃(SbW₉O₃₃)₂(H₂O)₃]¹²⁻ POM towards OER in neutral conditions and as a homogeneous catalyst. The tested POM presented good overall stability properties and a Tafel slope of 113 mV/dec, and it was demonstrated that the POM acted as the real catalyst in the OER conditions (Yu et al., 2018).

Table 4 summarizes the discussed POM-based electrocatalysts and their main OER performance parameters.

3 Oxygen reduction reaction (ORR)

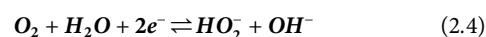
The ORR converts molecular oxygen to water via electron acceptance, which can occur through a 4e⁻ direct formation path or through a two-step 2e⁻ pathway that produces a peroxide as an intermediate. Similar to the OER, there are slight differences in the reaction intermediates when the reaction proceeds in alkaline media *versus* when it proceeds in acidic media, as shown below in equations 2.3 through 2.8 for:

Alkaline conditions

4e⁻ pathway:



2e⁻ pathway:

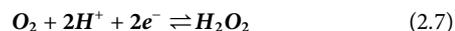


Acidic conditions

4e⁻ pathway:



2e⁻ pathway:



The main applications of ORR are in fuel cells and metal-air batteries, occurring during discharge at the cathode. Like OER, it presents sluggish kinetics and thus requires high overpotentials (Horn et al., 2021), emphasizing the need for highly active electrocatalysts. Furthermore, from an ideal perspective, the electrocatalyst would be bifunctional, i.e., it would also show good activity towards OER, as the reaction occurs during the charging process in these applications.

Generally, the 4e⁻ pathway is preferred because it has higher reaction kinetics and efficiency (Lu et al., 2019). Additionally, peroxide formation is avoided, which is particularly critical because it is a strong oxidant that can lower the electrode performance over time and damage the structure of fuel cells via degradation of the polymer electrolyte membrane (Lee and Popov, 2007). However, the 2e⁻ pathway can be preferred if the objective is peroxide production, since the electrochemical process may be more cost-effective than conventional technologies (Zheng et al., 2021).

The best metal electrocatalyst for ORR is Pt, as it shows high activity and selectivity towards the 4e⁻ pathway. However, Pt is scarce (more than gold and silver) (Zhang C. et al., 2017), and thus an expensive noble metal, while also having durability issues, especially when Pt-based materials are concerned (Zhang C. et al., 2017; Lu et al., 2019). This encourages researchers to seek out more cost-effective, highly active, and durable electrocatalysts based on cheaper and earth-abundant early transition metals (Ni, Co, Cu, Mn, etc.) to make these applications economically viable at an industrial scale.

3.1 Transition metal oxides for ORR

Cui et al. prepared porous NiO/NiCo₂O₄ nanotubes and tested their activity for the ORR in alkaline conditions (0.1 M KOH). The prepared composite performs similarly to state-of-the-art Pt/C electrocatalysts, having close onset potentials but with the oxides having a higher limiting current density. Additionally, the tested electrocatalyst showed higher stability than Pt/C (87% of current retention after 40,000 s vs 70% for Pt/C) and exhibited resistance to methanol crossover. The obtained Tafel slope was 61.8 mV/dec, and the reaction mechanism followed the 4e⁻ direct reduction path. The activity was attributed to the unique porous tubular structure with homogeneous oxide distribution along the surface (Cui et al., 2014).

Sidhureddy et al. disclosed the synthesis of Ni_xCo_{3-x}O₄ mesoporous spinel nano-oxides with different morphologies based on the Ni/Co ratio and tested their activities towards the ORR in alkaline electrolyte (0.1 M KOH). The best-performing sample, NCO-1 (1:2.06 Ni/Co ratio), presented an onset potential of 0.9 V vs RHE and was three times more active than its mono-metal oxide counterparts, while also exhibiting great tolerance to

methanol crossover (higher than benchmark Pt/C electrocatalyst), good general stability (94% current retention after 300 min) and a selective 4e⁻ reduction pathway. The performance was attributed to the abundance of octahedral site cations and defective oxygen sites in the structure (Sidhureddy et al., 2019).

Liu and Qin tested graphene-supported β-MnO₂ nanoparticles (MnO_x/graphene) for the ORR using an alkaline electrolyte (6 M KOH). The composite showed a Tafel slope of 91 mV/dec and an average number of exchanged electrons of 2.5, meaning that the composite was more selective towards the 2e⁻ peroxide forming path. The activity was attributed to the synergistic interactions between MnO₂ and graphene sheets (Liu and Qin, 2015).

Swetha et al. designed manganese oxide samples with different morphologies (nanowires, nanoflowers, and nanoparticles) and tested them towards the ORR in alkaline medium (0.1 M KOH). The best-performing Mn oxide morphology was the nanowire structure, which showed an onset potential of 0.83 V vs RHE and a 1.75 mA/cm² current density. This increased activity was attributed to the higher surface area contained by the nanowire structure, which increases active site exposition (Swetha et al., 2018).

Draskovic and Wu tested a series of cuprous delafossite oxides (CuBO₂; B = Sc, Y, La) supported on carbon black towards the ORR in an alkaline electrolyte (0.1 M KOH). The results demonstrated superior activity in the presence of carbon support. The oxides exhibited similar onset potentials and diffusion limiting currents, with a number of exchanged electrons in the range of 2.1–2.2 for CuScO₂ and CuYO₂ and in the range of 2.3–2.9 for CuLaO₂, indicating that the first two oxides prefer the 2e⁻ peroxide pathway while CuLaO₂ tends for the 4e⁻ pathway. In addition, the samples had Tafel slopes of -59, -55, and -56 mV/dec for CuScO₂, CuYO₂, and CuLaO₂ (Draskovic and Wu, 2017).

Saianand et al. reported the use of dispersed Cu/CuO nanospecies on mesoporous fullerenes (Cu-MFC₆₀) samples for the ORR in alkaline conditions (0.1 M KOH). The optimized electrocatalyst, Cu(15%)-MFC₆₀, presented an onset potential of 0.86 V vs RHE, a half-wave potential of 0.76 V vs RHE a diffusion limiting current density of -5.18 mA/cm², Tafel slope of 82 mV/dec, high selectivity towards the 4e⁻ transfer path, and improved stability, a performance comparable to that of benchmark commercial Pt/C electrocatalyst. The activity of the composite was attributed to the well-defined mesoporous features, abundant active sites, moderate surface area, and synergistic interactions between the metal and the support matrix (Saianand et al., 2020).

Table 5 compares the ORR performance parameters for the discussed oxide-based electrocatalysts.

3.2 Transition metal alloys for ORR

Sun et al. disclosed the synthesis and use of a 3D low-cost Co₃Fe₇ nanoparticles/nitrogen, manganese-codoped porous carbon (Co₃Fe₇/N, Mn-PC) as an ORR electrocatalyst in an alkaline electrolyte (0.1 M KOH). The composite material exhibited an onset and half-wave potential of 0.98 and 0.87 V and a Tafel slope of 86.9 mV/dec, outperforming the mono and bimetallic counterparts and the benchmark Pt/C electrocatalyst. Additionally, the average number of exchanged electrons was

TABLE 5 ORR electrocatalysts and their key performance indicators: transition metal oxides.

Electrocatalyst	Onset potential (V vs RHE)	Tafel slope (mV/dec)	Number of exchanged e ⁻	Electrolyte	Source
NiO/NiCo ₂ O ₄ nanotubes	0.92	61.8	3.9	0.1 M KOH	Cui et al. (2014)
NCO-1	0.90	-	3.96	0.1 M KOH	Sidhureddy et al. (2019)
MnO _x /graphene	-	91	2.5	6 M KOH	Liu and Qin (2015)
MnO _x nanowires	0.83	-	-	0.1 M KOH	Swetha et al. (2018)
CuScO ₂	-	59	2.1–2.2	0.1 M KOH	Draskovic and Wu (2017)
CuYO ₂	-	55	2.1–2.2	0.1 M KOH	Draskovic and Wu (2017)
CuLaO ₂	-	56	2.3–2.9	0.1 M KOH	Draskovic and Wu (2017)
Cu(15%)-MFC ₆₀	0.86	82	3.99	0.1 M KOH	Saianand et al. (2020)

TABLE 6 ORR electrocatalysts and their key performance indicators: transition metal alloys.

Electrocatalyst	Onset potential (V vs RHE)	Half-wave potential (V vs RHE)	Tafel slope (mV/dec)	Number of exchanged e ⁻	Electrolyte	Source
Co ₃ Fe ₇ /N, Mn/PC	0.98	0.87	86.9	4.01	0.1 M KOH	Sun et al. (2021)
Co _{0.5} Mo _{0.5} N _y /NCNCs	0.81	-	-	3.65–3.85	0.5 M H ₂ SO ₄	Sun et al. (2015)
NiCoSn	0.80	0.72	-	3.9	1 M KOH	Sajeew et al. (2023)
50 nm CuPd tetrapod	-	0.90	54	4	0.1 M KOH	Zhang L. et al. (2018)

4.01, and impressive methanol crossover resistance and stability were exhibited (i.e., current almost unchanged after adding 1 M CH₃OH and negative shift of 9 mV to the onset potential after 2,000 CV scans). The performance was attributed to a higher number of active sites and nitrogen ligands chelated with Fe and Co, increasing the charge transfer kinetics, and to the synergistic effects of Mn and N doping, which adjusted the electronic structure, thus favoring catalysis (Sun et al., 2021).

Sun et al. studied Mo-Co alloyed nitrides supported on nitrogen-doped carbon nanocages (Co_xMo_{1-x}N_y/NCNCs) as an electrocatalyst for ORR in acidic medium (0.5 M H₂SO₄). The best-performing electrocatalyst, Co_{0.5}Mo_{0.5}N_y/NCNCs, combined the advantages of high activity of Co nitride and good stability of Mo nitride in acidic conditions, which translated into an onset potential of 0.81 V vs RHE, good selectivity to the 4e⁻ reduction pathway, high stability (>80% current retention after 100 h and immunity to methanol crossover). The activity was attributed to the cobalt active reaction sites, smaller particle size that inhibited agglomeration, thus exposing more sites, and the synergistic effects between the metals (Sun et al., 2015).

Sajeew et al. synthesized a trimetallic NiCoSn alloy and tested its electrocatalytic properties towards the methanol oxidation reaction and the ORR in alkaline medium (1 M KOH). Regarding the ORR, the trimetallic sample presented an onset

and half-wave potential of 0.80 and 0.72 V vs RHE, respectively. Additionally, it had good selectivity for the 4-electron reduction pathway and exhibited good stability under ORR conditions and during methanol crossover. The verified performance was attributed to a higher abundance of metal redox active sites, larger surface area, and enhanced electron transport (Sajeew et al., 2023).

Zhang L. et al. disclosed the use of 50 nm Cu/Pd tetrapod as an ORR electrocatalyst in alkaline medium (0.1 M KOH). The material exhibited a half-wave potential of 0.90 V vs RHE and a 54 mV/dec Tafel slope, performing closely to state-of-the-art Pt/C electrocatalyst. The reduction was verified to follow the 4e⁻ direct reduction mechanism, and accelerated durability tests showed excellent retention of both current and morphology after 10,000 cycles at ORR conditions. This performance was attributed to the synergistic effects of the alloy and sharp-tip effects, which enabled negative charge accumulation on Pd atoms at the tetrapod tips (Zhang L. et al., 2018).

Table 6 contains the performance indicators for the analyzed ORR alloy-based electrocatalysts. Transition metals tend to leach out of alloy catalysts under fuel cell operating conditions, causing a reduction of the catalytic activity for ORR (Lee and Popov, 2007). As such, other types of materials are also being investigated for this reaction, including MOFs and POMs.

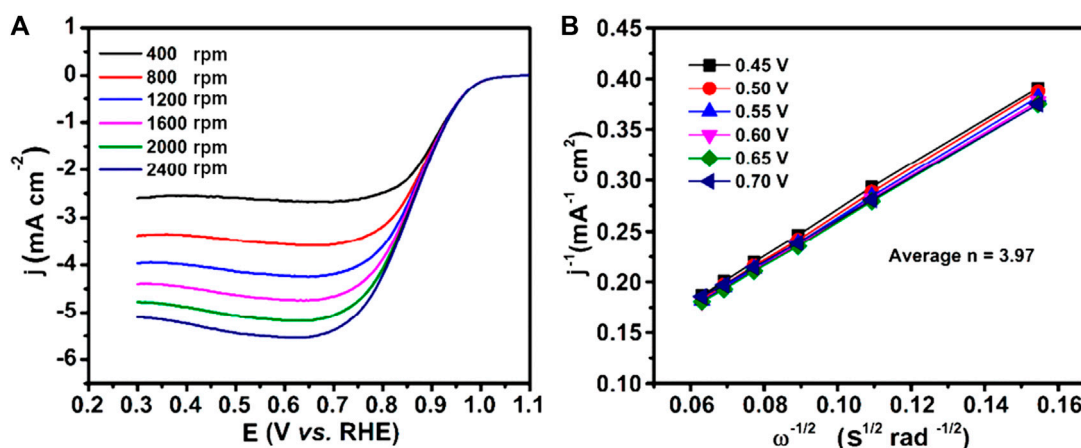


FIGURE 6

(A) Steady-state voltammograms of the ORR profiles at Cu@Cu₂O core-shell nanocatalyst in O₂-saturated 0.1 M KOH solution at different rotation rates and scan rate of 20 mV/s and (B) the corresponding Koutecky–Levich (K–L) plots (adapted from Kim et al., 2018).

3.3 Transition MOFs and MOF-derived electrocatalysts for ORR

Qin et al. designed a series of nanocomposites derived from bimetallic iron/nickel MOFs and nitrogen-doped graphene denoted as Fe/Ni-MOFs/NG, which was tested in alkaline electrolyte for the ORR (0.1 M KOH). The best performance was shown by Fe/Ni-MOF/NG-20, which had an onset potential of 1.09 V, exchanged an average of 3.93 electrons, a Tafel slope of 58.2 mV/dec, methanol crossover resistance, and good stability features at ORR conditions. The performance was attributed mainly to the unique structure, which has Fe/Ni-MOF acting as catalyst and NG acting as cocatalyst, and high exposed surface area due to the hierarchical porous structure (Qin et al., 2019).

Rehman et al. synthesized Ni-N carbon nanotubes (Ni-N-CNTs) derived from ZIF-8 MOF crystals and tested their activities for ORR at alkaline conditions (0.1 M KOH). The electrocatalyst presented an onset and half-wave potential of 0.87 and 0.75 V vs RHE, a Tafel slope of 84 mV/dec, a transferred number of electrons around 3.9, and good stability properties. It also presented a -5.51 mA/cm^2 limiting-current density, outperforming state-of-the-art Pt/C electrocatalyst, which showed a limiting-current density of -5.2 mA/cm^2 (Rehman et al., 2022).

Tong et al. reported the synthesis of a series of cobalt nanoparticles/N-doped carbon catalysts derived from ZIF/CNT nanonecklaces and tested their use for the ORR in alkaline electrolyte (0.1 M KOH). The best-performing sample had an onset potential of 0.92 V vs RHE, exchanged 4 electrons during the reaction, and showed good stability after 1,000 cycles at ORR conditions. The verified performance was attributed to the synergistic effect of cobalt content and the well-dispersed one-dimensional structure (Tong et al., 2020).

Feng et al. developed a N-doped porous graphitized carbon-supported cobalt disulfide derived from ZIF-67 MOF and tested its activity towards ORR in alkaline conditions (0.1 M KOH). The sample showed an onset and a half-wave potential of 0.86 and 0.79 V vs RHE, a Tafel slope of 56 mV/dec, and a number of transferred

electrons in the 3.62–3.72 range, exhibiting similar performance to the benchmark Pt/C ORR electrocatalyst, while showing better stability properties in methanol crossover conditions and after prolonged exposure to ORR conditions (1,000 cycles). The performance was attributed to N-doping, enhanced conductivity given by the porous graphitized carbon support, and the presence of active N-Co sites (Feng et al., 2019).

Mani et al. produced a Cu-based MOF [(Cu₄Cl)₃(H_{0.5}BTT)₈(H₂O)₁₂]-3MeOH-9DMF with tetrazole ligand (H₃BTT = 5,5'-(1,4-phenylene) bis(1H-tetrazole)) and tested its performance in alkaline medium (0.05 M KOH). The MOF showed an onset and half-wave potential of 0.94 and 0.78 V vs RHE, a number of transferred electrons of approximately 4, exceptional methanol crossover (no changes after addition of 1 M MeOH), and good cycling stability (84% of current retained after 12 h), with no changes to the porous morphology detected after ORR. The high activity was attributed to the formation of nascent copper(I) moiety from copper (II), which is also surrounded by nitrogen-rich tetrazole moiety, thus increasing ORR activity (Mani et al., 2019).

Kim et al. reported the use of a Cu(II)-MOF-derived Cu@Cu₂O core-shell nanocatalyst obtained via reduction with borohydride as an electrocatalyst for the ORR in alkaline medium (0.1 M KOH). The material presented an onset and half-wave potential of 0.93 and 0.86 V vs RHE, and an average of 3.97 electrons exchanged, as shown in Figure 6, thus demonstrating good selectivity towards the preferred ORR pathway. The activity was attributed to the synergistic morphological effects of the core-shell structure, high dispersion of Cu₂O, and strong adsorption of O₂ on the catalyst surface (Kim et al., 2018).

Table 7 compiles the key ORR performance parameters for the MOF and MOF-derived electrocatalysts shown in this section.

3.4 Transition metal POMs for ORR

Zhang S. et al. designed a series of carbonaceous supported (thermalized triazine-based frameworks (TTF), fluorine-doped TTF (TTF-F), reduced graphene oxide or carbon Vulcan XC-72)

TABLE 7 ORR electrocatalysts and their key performance indicators: transition MOFs and MOF-derived electrocatalysts.

Electrocatalyst	Onset potential (V vs RHE)	Half-wave potential (V vs RHE)	Tafel slope (mV/dec)	Number of exchanged e ⁻	Electrolyte	Source
Fe/Ni-MOF/NG-20	1.09	-	58.2	3.925	0.1 M KOH	Qin et al. (2019)
Ni-N-CNTs	0.87	0.75	84	3.9	0.1 M KOH	Rehman et al. (2022)
ZIF/CNT-800-AL (Zn/Co = 2/8)	0.92	-	-	4	0.1 M KOH	Tong et al. (2020)
CoS ₂ @NC	0.86	0.79	56	3.62–3.72	0.1 M KOH	Feng et al. (2019)
[(Cu ₄ Cl) ₃ (H _{0.5} BT) ₈ (H ₂ O) ₁₂].3MeOH.9DMF	0.94	0.78	-	4	0.05 M KOH	Mani et al. (2019)
Cu@CuO ₂ core-shell	0.93	0.86	-	3.97	0.1 M KOH	Kim et al. (2018)

precious-metal free POMs (based on Ni, Co, and Cu) and tested their activities for ORR in alkaline medium (0.1 M KOH). The best-performing composite, Cu₆Ni₇/TTF-F, presented an onset potential of 0.91 V vs RHE and had an electron transfer number in the 3.92–3.94 range, while also presenting excellent stability (negligible changes after 6,000 cycles). They also tested the influence of the POM-core in the electrocatalyst, concluding that the Ni and Cu-based POMs (either individually or having both metals in the POM) induce higher activity when compared to the Co-POMs (Zhang S. et al., 2017).

Zheng et al. produced a new Ni-POM compound, NiP₄Mo₆, and later vulcanized it, testing both materials' electrocatalytic activity towards the ORR in alkaline conditions (0.1 M KOH). The materials presented different selectivities for the ORR, with NiP₄Mo₆ being selective to the 4e⁻ path and its vulcanized counterpart being selective to the 2e⁻ path. The vulcanized material also presented higher half-wave potential and lower Tafel slope: 0.77 and 0.73 V vs RHE, and 98.1 and 106.2 mV/dec, respectively, for vulcanized and unvulcanized samples. Both materials also presented excellent stability with virtually no change after 8,000 cycles. The change in the ORR mechanism was attributed to the vulcanization process, which substituted O²⁻ atoms with S²⁻ atoms, affecting the adsorption energies, thus weakening it in such a way that H₂O₂ production would be favored (Zheng et al., 2021).

Sanji et al. reported the use of a POM-modified Pd₈Ni₂/rGO (Pd₈Ni₂/rGO-POM) as an ORR electrocatalyst in alkaline conditions (0.1 M KOH). It presented an onset potential of ~0.83 V vs RHE, a Tafel slope of 59.8 mV/dec, and an average of 3.9 electrons exchanged during the ORR. Furthermore, the composite exhibited excellent methanol crossover tolerance and better current retention properties after 10 h at ORR conditions, outperforming the Pt/C state-of-the-art electrocatalyst. Lastly, the performance was attributed to the Pd-Ni alloy interaction (their interactions modify their electronic structures, contributing to enhanced ORR performance), the rGO support (improves conductivity and mass transfer), and the synergistic effects between them and the POM (Sanji et al., 2021).

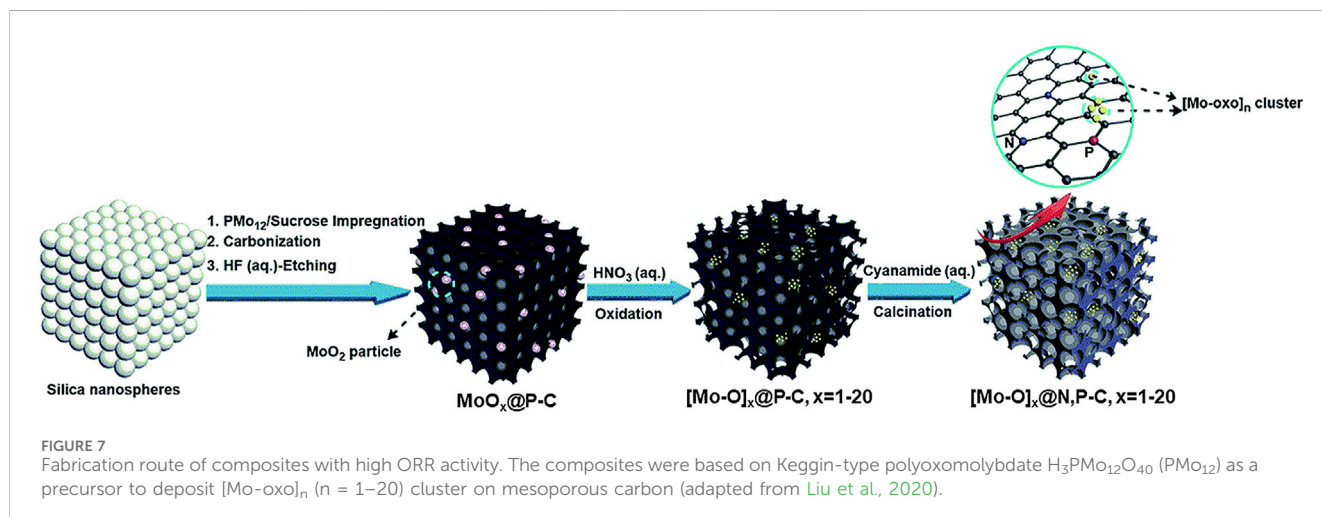
Ammam et al. performed cyclic voltammetry tests on the Mn-substituted dissymmetrical Dawson-sandwich type and the Keggin

sandwich banana-shaped POMs, [Mn^{II}₄(H₂O)₂(H₄AsW₁₅O₅₆)₂]¹⁸⁻ and [(Mn^{II}OH₂)Mn^{II}PW₉O₃₄]₂(PW₆O₂₆)¹⁷⁻ (Mn₄As₂W₃₀ and Mn₆P₃W₂₄). Subsequently, they evaluated their activity towards the ORR at pH 5 and pH 3, respectively. The results indicated that both catalysts demonstrated activity towards the ORR, but a deposited layer of Mn oxides (mainly MnO₂) acted as the true catalyst. This was further corroborated by performing additional CV cycles, revealing an increase in the thickness of the oxide layer and a corresponding enhancement in ORR activity (Ammam et al., 2011).

Fernandes et al. disclosed the use of the Co-based sandwich (TBA)₇H₃[Co₄(H₂O)₂(PW₉O₃₄)₂] POM, TBA-Co₄(PW₉)₂, supported on different carbon-based materials such as single-walled carbon nanotubes (SWCNT), graphene flakes (GF), nitrogen-doped carbon nanotubes (N-CNT), and nitrogen-doped few-layer graphene (N-FLG), as ORR electrocatalysts in alkaline medium (0.1 M KOH). The electrocatalysts had onset potentials ranging from 0.77 to 0.9 V vs RHE, Tafel slopes ranging from 68 to 96 mV/dec, and electron exchange numbers ranging from 2.7 to 4. POM@N-CNT is shown to have an activity that surpasses the state-of-the-art Pt/C electrocatalyst. Additionally, the electrocatalysts presented a cyclic stability similar to that of commercial Pt/C and much higher methanol stability. Lastly, all composite materials performed better than their isolated supports, with Co₄(PW₉)₂@N-CNT catalytic activity outperforming Pt/C (Fernandes et al., 2018a).

Song et al. confined a cobalt-centered POM, [CoPW₁₂]⁶⁻, in the void space of the ZIF-8 MOF and later prepared a Co-POM@MOF-derived N-doped porous carbon composite via pyrolysis treatment to test its performance towards ORR in alkaline electrolyte (0.1 M KOH). The material presented a half-wave potential of 0.84 V vs RHE, a Tafel slope of 63 mV/dec, an electron transfer number of 4.1, and good stability properties (retains activity after 1,000 cycles) (Song et al., 2022).

Rousseau et al. synthesized a noble metal-free Co/Zn POM complex supported on Vulcan carbon XC-72 (Co₇Zn/C) and tested its activity towards the ORR in alkaline medium (0.1 M KOH). The material had an electron exchange number between 3.6 and 4, signifying its selectivity towards the 4e⁻ reduction path. It presented activity comparable to commercial Pt/C, showing higher stability after 11 h at ORR conditions and much higher



methanol crossover tolerance. The material also showed good activity in neutral medium, compared to commercial Pt/C, but with higher stability (Rousseau et al., 2015).

Liu et al. disclosed a top-down approach to deposit POM-like metal oxo clusters by using the solution-stable Keggin-type polyoxomolybdate $H_3PMo_{12}O_{40}$ (PMo_{12}) as a precursor to deposit $[Mo-oxo]_n$ ($n = 1-20$) cluster on mesoporous carbon, synthesizing three different composites, whose synthesis processes are presented schematically in Figure 7. Their electrocatalytic activity for the ORR in alkaline electrolyte (0.1 M KOH) was tested. The composites had an onset potential in the range of 0.75–0.93 V vs RHE, Tafel slopes in the range of 44.2–109 mV/dec, and the first two composites favored the $2e^-$ reaction path, while the third composite favored the $4e^-$ reaction pathway. Additionally, the third composite demonstrated an activation behavior during chronoamperometric tests to determine its stability, showing an increase in current after 20 h and no further changes after a total period of 50 h, and demonstrated high methanol crossover tolerance, outperforming the commercial Pt/C electrocatalyst both in activity and stability. The activity was attributed to good dispersion of the $[Mo-oxo]_n$ clusters, high surface area, and N-doping of the carbon substrate (Liu et al., 2019).

Zhao et al. combined a lacunary Keggin POM cluster, $[PW_{11}O_{39}]^{7-}$, with 3D ordered microporous graphitic carbon nitride (3DOM g- C_3N_4) to generate an electrocatalyst with favorable selectivity for the 2 electrons ORR pathway, testing it electrochemically on neutral medium and via light-driven reaction. The synthesized composite showed activity for the light-driven production of H_2O_2 , with a production rate of 2.4 $\mu\text{mol/h}$, and electrochemical tests demonstrated that it had an electron transfer number around 2.3, indicating its selectivity towards the intended ORR mechanism (Zhao et al., 2017).

Table 8 summarizes the ORR performance parameters for the discussed POM-based electrocatalysts.

4 Hydrogen evolution reaction (HER)

The HER is the cathodic reaction occurring in water electrolysis. The HER kinetics differ according to pH: at acidic conditions, it has higher kinetics, while in alkaline and neutral conditions, it has

slower kinetics (around 2 to 3 orders of magnitude slower), constituting a disadvantage for alkaline water electrolysis technologies. The reason lies in the inherent HER mechanism, which differs from acid to alkaline/neutral conditions (Chatenet et al., 2022; Pratama et al., 2023), as shown in Figure 8.

Interestingly, the choice of alkaline electrolytes relative to acidic ones for water electrolysis comes down to the high cost of noble metal electrode materials and equipment limitations, since acid conditions cause equipment corrosion, lowering its lifetime (Zeb et al., 2023). Additionally, the reaction products, akin to OER and ORR, change slightly depending on the pH, as can be seen in equations 2.9 and 2.10 for acidic and neutral/alkaline medium, respectively:



Furthermore, the inherent HER mechanism only involves two electron transfers, meaning it has fewer thermodynamic demands (resulting in a lower activation barrier) (Horn et al., 2021; Chatenet et al., 2022). Thus, lower overpotentials are generally needed to reach reasonable reaction rates compared to the OER.

Regarding the state-of-the-art electrocatalysts, the one with the highest performance is, akin to ORR, commercial Pt/C, which shows the ideal adsorption energies (not too high and not too low), and thus presents high performance for the HER (Chatenet et al., 2022; Zeb et al., 2023). However, given the noble nature of Pt, it is an expensive and scarce material, and this limits the potential for large-scale applications due to cost-related reasons, meaning that much interest and investment has been applied in the discovery of stable, low-cost, and high-performance alternative electrocatalysts, generally based on early transition metals such as Ni, Mn, Co, and Cu.

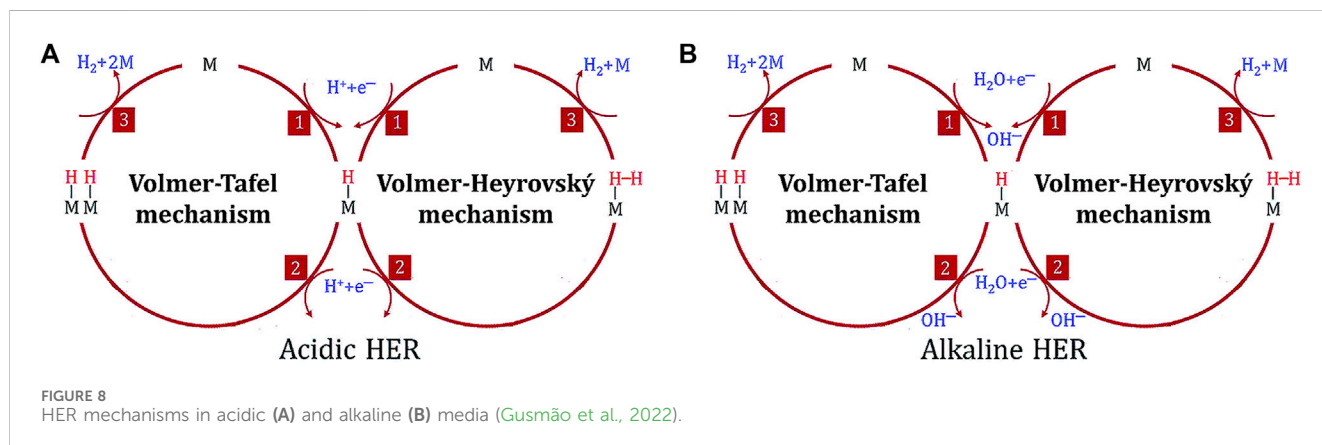
4.1 Transition metal oxides for HER

Mukherjee et al. designed a reduced graphene oxide embedded nickel ferrite oxide (rGO-NiFe₂O₄) and tested its electrocatalytic activity for the HER in acidic medium (0.5 M H₂SO₄). The observed

TABLE 8 ORR electrocatalysts and their key performance indicators: transition metal POMs.

Electrocatalyst	Onset potential (V vs RHE)	Tafel slope (mV/dec)	Number of exchanged e ⁻	Electrolyte	Source
Cu ₆ Ni ₇ /TTF-F	0.91	-	3.92–3.94	0.1 M KOH	Zhang S. et al. (2017)
NiP ₄ Mo ₆	-	98.1	3.86–3.88	0.1 M KOH	Zheng et al. (2021)
S-NiP ₄ Mo ₆	-	106	2.02–2.08	0.1 M KOH	Zheng et al. (2021)
Pd ₈ Ni ₂ /rGO-POM	0.83	59.8	3.9	0.1 M KOH	Sanji et al. (2021)
Co ₄ (PW ₉) ₂ @N-CNT	0.90	92	4	0.1 M KOH	Fernandes et al. (2018a)
Co ₄ (PW ₉) ₂ @SWCNT	0.77	68	3.9	0.1 M KOH	Fernandes et al. (2018a)
Co ₄ (PW ₉) ₂ @GF	0.89	71	2.7	0.1 M KOH	Fernandes et al. (2018a)
Co ₄ (PW ₉) ₂ @N-FLG	0.89	63	3.6	0.1 M KOH	Fernandes et al. (2018a)
Co-W-NC	-	63	4.1	0.1 M KOH	Song et al. (2022)
Co-Zn/C	-	-	3.6–4	0.1 M KOH	Rousseau et al. (2015)
MoO _x @P-C	0.75	109	2	0.1 M KOH	Liu et al. (2020)
[Mo-O] _x @P-C, X = 1–20	0.88	68.1	2	0.1 M KOH	Liu et al. (2020)
[Mo-O] _x @N,P-C, X = 1–20	0.93	44.2	3.8–3.9	0.1 M KOH	Liu et al. (2020)
3DOM g-C ₃ N ₄	-	-	2.3	0.1 M PBS ^a	Zhao et al. (2017)

a) PBS, phosphate buffer solution.



onset overpotential and the necessary overpotential to achieve current densities of 10, 30, and 100 mA/cm² were 5, 42, 87, and 158 mV, respectively. Additionally, the obtained Tafel slope was 58 mV/dec. The electrocatalyst also presented great stability, with virtually no change in the cathodic current after 5,000 cycles and a stable current after 12 h of operation at HER conditions. The activity was attributed to the strong chemical-electronic coupling between rGO and NiFe₂O₄, the formation of non-agglomerated small nanoparticles, and the creation of oxygen vacancies in the electrocatalyst structure (Mukherjee et al., 2018), Chu et al. prepared and tested a hybrid Ni/NiO@C/GR-t-w (derived from the carbonization of Ni-MOF-74 and graphene oxide composites at different temperatures (t) and with different graphene oxide

contents (w)) for the HER reaction in acid electrolyte (0.5 M H₂SO₄). The best-performing sample, Ni/NiO@C/GR-900-8, presented an onset potential of -34.7 mV vs RHE and an overpotential of 108 mV to reach 10 mA/cm², a Tafel slope of 44 mV/dec, and good stability properties, with no observed relevant change after 24 h of operation at 10 mA/cm² and after 1,000 HER cycles. The performance was attributed to the synergistic interactions at the Ni/NiO interface and the high surface area due to graphene incorporation (Chu et al., 2018).

Zeng et al. synthesized a series of NiMnO oxides with differing structures by adjusting the crystallization process via the addition of polyethylene glycol (PEG) in varying quantities and tested their properties towards the HER in alkaline medium (1 M KOH). The

best-performing oxide was NMO-PEG-3g, which presented an onset potential of -36.3 mV vs RHE and an overpotential of 140 and 256 mV to reach 10 and 100 mA/cm², respectively. Additionally, it presented a Tafel slope of 94 mV/dec, great stability properties with stable current after 24 h of HER, and activation with increased activity after 2,000 cycles. The enhanced performance was attributed to the petal-like scales in the structure, which increased surface area and thus exposed more active sites (Zeng et al., 2020).

Huang et al. produced a nanosized spinel Co-Mn oxide strongly coupled with ultrathin Ti₃C₂T_x MXene nanosheets (MnCo₂O₄/Ti₃C₂T_x) with different oxide loadings and tested its electrocatalytic potential toward the HER in acidic medium (0.5 M H₂SO₄). The best-performing sample had 50% oxide content, presented an onset overpotential of 51 mV, an overpotential to reach 10 mA/cm² of 177 mV, and a Tafel slope of 79 mV/dec, along with good stability and cyclic properties (nearly unchanged current after 16 h of operation and after 2,000 cycles). The activity was attributed to high electric conductivity and electronic structure optimization due to the incorporation of MXene nanosheets, thus enhancing the intrinsic catalytic activity and higher surface area with more exposed active sites (Huang et al., 2022).

Wu Y. et al. reported the synthesis of octahedral cobalt oxide particles via a hydrothermal method and tested its capacities towards catalyzing the HER in basic medium (1 M KOH). The material presented an overpotential of 112 mV to achieve 20 mA/cm², and a Tafel slope of 94 mV/dec. It also had good cyclic and stability properties, with little observed difference after 2,000 cycles and after 20 h of operation. The activity was attributed to a higher surface area, which exposes more active sites (Wu Y. et al., 2020).

Flores-Lasluisa et al. studied the Cu-doping of Co spinel oxides supported on high porosity activated carbon and their activity for the HER electrocatalysis in alkaline medium (0.1 M KOH). The obtained results indicate that the best-performing sample, AC-CuCo₂O₄, presented a Tafel slope of 300 mV/dec and -14.6 mA/cm² for 400 mV of overpotential. The higher activity was attributed to better particle agglomeration control and higher electrical conductivity caused by the supporting activated carbon, substitution by Cu atoms at the octahedral position, and a higher number of oxygen vacancies and Co³⁺ sites, creating synergistic effects that enhanced catalytic activity (Flores-Lasluisa et al., 2019).

Muralikrishna et al. disclosed the production of graphene oxide and Cu hybrid (GO-Cu²⁺) by controlling pH and Cu²⁺ concentrations during synthesis. They tested their ability to electrocatalyze the HER in an acidic medium (0.1 M H₂SO₄). The results indicated that the optimal synthesis was done at neutral pH and with a concentration of 30 mM of Cu²⁺. The hybrids had Tafel slopes around 120 mV/dec, along with moderate cyclic properties, with a brief reduction in current after 100 cycles (Muralikrishna et al., 2015).

Katubi et al. evaluated the performance of a hybrid nanocomposite comprising mixed metal oxides (Cu and W) and reduced graphene oxide (WO₃/CuO/rGO nanohybrid) towards HER in alkaline medium (1 M KOH). The composite presented an overpotential of 400 mV to achieve 200 mA/cm² and a Tafel slope of 44 mV/dec, along with good stability properties showing only a slight reduction in current after 12 h of operation, outperforming the unsupported and mono-metallic oxide counterparts. The verified activity was attributed to the high conductivity of rGO, higher number of exposed catalytic sites, and the synergistic interactions between the WO₃ and CuO nanoparticles (Katubi et al., 2023).

Table 9 condenses the performance indicators for the discussed oxide-based HER electrocatalysts.

4.2 Transition metal alloys for HER

Zhang et al. designed porous nickel-supported nanostructured Ni-Co electrodes with different morphologies that depended on the electrodeposition current and tested their activities towards the HER in alkaline electrolyte (1 M KOH). The results demonstrated that the best-performing morphology were the Ni-Co nanocones, which presented an onset potential of -14 mV vs RHE, an overpotential of 86.7 mV to achieve 10 mA/cm², and a Tafel slope of 69.8 mV/dec. Additionally, catalyst morphology was unchanged, and the overpotential to reach 10 mA/cm² only increased slightly after 10 h of operation at HER conditions. Finally, the activity was attributed to the synergism between the catalytic properties of Ni and Co, and the hierarchical morphology and sharp edges structure (Zhang et al., 2019).

Cao et al. fabricated radially aligned NiMo alloy microtubes on nickel foam (NiMo MT/NF) and verified its performance towards the HER in basic conditions (1 M KOH). The electrocatalyst

TABLE 9 HER electrocatalysts and their key performance indicators: transition metal oxides.

Electrocatalyst	η_{10} (mV)	Tafel slope (mV/dec)	Electrolyte	Source
rGO-NiFe ₂ O ₄	42	58	0.5 M H ₂ SO ₄	Mukherjee et al. (2018)
Ni/NiO@C/GR-900-8	108	44	0.5 M H ₂ SO ₄	Chu et al. (2018)
NMO-PEG-3g	140	94	1 M KOH	Zeng et al. (2020)
MnCo ₂ O ₄ /Ti ₃ C ₂ T _x	177	79	0.5 M H ₂ SO ₄	Huang et al. (2022)
Octahedral CoO _x particles	112@20 mA/cm ²	94	1 M KOH	Wu Y. et al. (2020)
AC-CuCO ₂ O	-	300	0.1 M KOH	Flores-Lasluisa et al. (2019)
GO-Cu ²⁺	-	120	0.1 M H ₂ SO ₄	Muralikrishna et al. (2015)
WO ₃ /CuO/rGO nanohybrid	400@200 mA/cm ²	44	1 M KOH	Katubi et al. (2023)

presented an overpotential of 119 mV to reach 10 mA/cm² and a Tafel slope of 119 mV/dec. Additionally, the material shows good cyclic and stability properties, since a negligible current density is lost after 1,000 cycles, and it can retain its activity for at least 10 h. The verified performance is attributed to a higher number of active sites and facilitated electron transport because of the unique tubular structure and low boundary resistance (Cao et al., 2019).

Liu et al. synthesized Ni-Mn-P electrocatalysts via electrochemical deposition method and tested their abilities towards HER catalysis in a basic electrolyte (1 M KOH). The results demonstrated that the best sample presented an overpotential of 113 mV to achieve 10 mA/cm² and a 74 mV/dec Tafel slope. Additionally, good stability properties were verified since the structural integrity was maintained after 20 h of HER operation (at 10 mA/cm² and 60 mA/cm²), and only a slight current drop was observed. The activity was attributed to Mn doping, which promoted the formation of a coral structure, and the synergistic effects between Ni, Mn, and P (Liu et al., 2021).

Ge et al. used Mn metal as a dopant to enhance the HER activity of urchin-like CoP electrocatalysts at alkaline and acidic media (1 M KOH and 0.5 M H₂SO₄). The results demonstrated that the best performance in both media was attained by the sample with 15 wt% Mn. Accordingly, the overpotentials needed to reach 10 mA/cm² were 100 and 65 mV, and Tafel slopes were 53 and 32 mV/dec, respectively, in alkaline and acid conditions, thus performing closely to benchmark Pt/C electrocatalyst and outperforming pristine CoP. Additionally, after 20 h of operation, the electrocatalyst showed a very small increase in overpotential (2.4 mV and 1.1 mV for alkaline and acid media, respectively) at 10 mA/cm² and no morphological changes, thus demonstrating good stability properties. The observed activity was attributed to a reduction in the hydrogen adsorption energy with the Mn doping, which enhanced the HER rate (Ge et al., 2018).

Wang H. et al. proposed preparing a nitrogen-doped porous carbon-supported cobalt material with a high graphitization degree and different dispersant content as a HER electrocatalyst in alkaline medium (1 M KOH). The best-performing sample, Co@NPC-F4, exhibited an overpotential of 259 mV to achieve 10 mA/cm² and a Tafel slope of 99 mV/dec. It also showed good stability properties, retaining 83% of current after 6 h of operation. The performance was attributed to the high surface area of the NPC and the optimization of the porous bundle structure during synthesis (Wang H. et al., 2019).

Guan et al. prepared Co-Ni alloys supported on N-doped carbon nanofibers via *in-situ* growth and tested their activity towards the HER in basic medium (1 M KOH). The material presented an 86 mV overpotential to reach 10 mA/cm² and a Tafel slope of 152.3 mV/dec, alongside good cyclic and stability properties, with almost no change in activity after 1,000 cycles and 25 h of operation, respectively, performing closely to the state-of-the-art Pt/C electrocatalyst. The enhanced activity is related to more useable active sites due to the N-doped carbon nanofibers' 3D structure, the NiCo alloy's synergistic effects, and the presence of smaller and more uniform alloy nanoparticles (Guan et al., 2021).

Butt et al. deposited a layer of metallic Cu on thermally synthesized CuO nanowires via a dielectric barrier discharge method and tested its performance towards the HER in 0.1 M K₂SO₄ electrolyte. The best-performing sample, Cu500 (indicating that the CuO synthesis temperature was 500°C), presented an overpotential of 210 mV to achieve 10 mA/cm², a Tafel slope of 178 mV/dec, and an exchange current density of 0.6 mA/cm², along with good stability properties after almost 4 h of operation. The performance was attributed to the presence of the metallic Cu nanowires alongside the CuO nanowires (Butt et al., 2021).

Shen et al. produced a series of Ni-Cu alloy nanoparticles encapsulated into graphitic shells with different shell thicknesses and tested their performances toward HER electrocatalysis in different pH values (0, 7, and 14). The catalysts showed, in general, better performance on acidic media, and the best-performing sample (NiCo@C-1) presented an overpotential of 48 mV to achieve 10 mA/cm² and a Tafel slope of 63.2 mV/dec under these conditions. Furthermore, accelerated durability tests demonstrated good cyclic properties, with virtually negligible differences after 2,000 HER cycles, and chronoamperometric tests showed good stability properties, with a current retention of around 63% and no structural changes. The performance was much better than the pristine NiCu alloy and closely resembled that of the benchmark Pt/C electrocatalyst. This was attributed to the interactions between the alloy and the carbon shell, which affected the electronic structure and adjusted the hydrogen adsorption energy to enhance activity (Shen et al., 2017).

Table 10 summarizes the performance indicators for the considered Alloy-based HER electrocatalysts.

TABLE 10 HER electrocatalysts and their key performance indicators: transition metal alloys.

Electrocatalyst	η_{10} (mV)	Tafel slope (mV/dec)	Electrolyte	Source
Ni-Co nanocones	86.7	69.8	1 M KOH	Zhang et al. (2019)
NiMo MT/NF	119	119	1 M KOH	Cao et al. (2019)
Ni-Mn-P	113	74	1 M KOH	Liu et al. (2021)
15Mn-CoP	100	53	1 M KOH	Ge et al. (2018)
15Mn-CoP	65	32	0.1 M H ₂ SO ₄	Ge et al. (2018)
Co@NPC-F4	259	99	1 M KOH	Wang H. et al. (2019)
Co-Ni/NCNFs	86	152.3	1 M KOH	Guan et al. (2021)
Cu500	210	178	0.1 M K ₂ SO ₄	Butt et al. (2021)
NiCO@C-1	48	63.2	acidic electrolyte	Shen et al. (2017)

4.3 Transition MOFs for HER

Dao et al. developed graphene-doped Ni-MOFs via the solvothermal method with different graphene contents and tested their HER electrocatalytic properties in alkaline electrolyte (1 M KOH). The best-performing sample, MOF(Ni)-GR(4%), needed an overpotential of 268 mV to reach 10 mA/cm² and had a Tafel slope of 108 mV/dec. Furthermore, chronopotentiometric tests indicated that the MOF catalyst had better stability than the benchmark Pt/C electrocatalyst, and the activity was attributed to a higher surface area, which contributed to exposing more active sites and to the better electronic conductivity of graphene, which facilitated charge transfer and thus enhanced HER catalysis (Dao et al., 2022).

Wu et al. designed Ni (II) based MOFs, [Ni(bib)₂(SO₄)_n]; bib = 1,4-bis(1-imidazolyl)benzene via hydrothermal method and calcination at different temperatures. These MOFs were tested for HER electrocatalysis in acid medium (0.5 M H₂SO₄). The best-performing sample, Ni-MOF-800, presented an overpotential of 356 mV to achieve 10 mA/cm² and a Tafel slope of 127.3 mV/dec. The catalyst stability was also tested, and it was verified that after 2,000 cycles, the HER activity was almost unchanged, and the morphology was completely intact. The performance was attributed to the enhanced conductive properties, which increased charge transfer kinetics and thus incremented HER rate (Wu et al., 2022).

Duan et al. prepared peony petal-like CoMnP nanoparticles supported on nickel foam via solvothermal growth route on CoMn-MOF-71 nanosheets and tested its HER electrocatalytic properties in acid and basic media (0.5 M H₂SO₄ and 1 M NaOH). The sample presented overpotentials of 66.6 and 53.9 mV to reach 10 mA/cm² and Tafel slopes of 38.8 and 63 mV/dec for acid and alkaline medium, respectively, which had close performance to Pt/C benchmark electrocatalyst. Additionally, in acid conditions, the current retention after 12 h only shows a small decrease, and the performance after 1,000 cycles slightly increased, while no morphological changes were observed after 1,500 cycles. The same results were observed for alkaline conditions. The enhanced performance was attributed to higher specific surface area, exposing more active sites and facilitating electrolyte diffusion, and to synergistic effects between Mn and Co that can modulate the electronic structure to optimize the adsorption energies and enhance the HER process (Duan et al., 2022).

Liu et al. described a phosphorization process to create carbon fiber paper-supported CoP species in a Co-MOF, thus originating a CoP/Co-MOF/CF hybrid, and tested its catalytic activity toward the HER in acidic (0.5 M H₂SO₄), neutral (pH 7 PBS buffer solution) and alkaline (1 M KOH) media. The overpotential needed to achieve a 10 mA/cm² was 27, 34, and 49 mV, and the Tafel slope was 43, 56, and 63 mV/dec, for acidic, basic, and neutral conditions, respectively, performing closely to the benchmark Pt/C electrocatalyst. Additionally, the material demonstrated good cyclic and stability properties in acid, neutral, and alkaline conditions, with negligible differences in performance after 2,000 cycles. It showed a slight morphology degradation in alkaline medium but remained intact in the other testing conditions. The performance was attributed to the electronic interactions of CoP and Co-MOF, which modulated H₂O and H adsorption energies to more optimal values, thus enhancing HER,

and to the MOF porous network, which exposes more active sites and facilitates gas release (Liu et al., 2019).

Pan et al. reported a method to develop a Co,N-doped graphitic carbon electrocatalyst (Co-MOF-800) based on a flower-like MOF ([Co(BIPA)(5-OH-bdc)](DMF)_n]; BIPA = bis(4-(1H-imidazole-1-yl) phenyl)amine and 5-OH-bdc = deprotonated 5-hydroxyisophthalic acid) and tested its HER electrocatalysis properties in acidic medium (0.5 M H₂SO₄). An onset potential of ca. -120 mV vs RHE, an overpotential of 193 mV to achieve 10 mA/cm², and a Tafel slope of 77.1 mV/dec were determined for those conditions, along with appreciable current retention after 20 h of operation and only a slight loss in performance after the elapsed time. The activity was attributed to synergistic interactions between Co and N, which optimized adsorption energies and modified the electronic structure of carbon, enhancing the HER rate (Pan et al., 2019).

Nivetha et al. synthesized a Meso-Cu-BTC MOF and tested its performance towards HER electrocatalysis in an alkaline electrolyte (1 M NaOH). The catalyst demonstrated an onset overpotential of 25 mV, an exchange current density of 6 mA/cm², and a Tafel slope of 33.4 mV/dec, but still underperformed the benchmark Pt/C electrocatalyst. After 1,000 cycles, there was no observable change in performance, confirming the good stability properties of the material. The observed activity was attributed to the highly porous network of the octahedral MOF, which enhanced electronic and ionic transfer, thus increasing the HER rate (Nivetha et al., 2020).

Zhang et al. disclosed the synthesis of three different porous MOFs based on different transition metals, Ni, Co, and Cu, and on H₃BTC (benzene-1,3,5-tricarboxylic acid), originating rhombic octahedral Cu-BTC, rod-shaped Co-BTC, and spherical Ni-BTC materials, which were tested towards HER electrocatalysis on acidic medium (0.5 M H₂SO₄). The materials presented an overpotential to reach 10 mA/cm² of 53, 123, and 270 mV and Tafel slopes of 62, 100, and 155 mV/dec for Ni-BTC, Co-BTC, and Cu-BTC, respectively, with Ni-BTC performing similarly to Pt/C state-of-the-art electrocatalyst. The MOFs demonstrated different stability properties, with Ni-BTC demonstrating no current retention drops and Co-BTC and Cu-BTC showing 60% and 72% current retention, although no structural or morphological changes were detected after the tests. The performance was attributed to structural features such as large surface area, porous and adjustable structure, and transition metal center regulation (Zhang et al., 2020).

Table 11 compiles the relevant HER performance parameters for the discussed MOF electrocatalysts.

4.4 Transition metal POMs for HER

Sun et al. prepared an electrocatalyst of Ni and Mo₂C nanoparticles painted with N-doped carbon layers (Ni/Mo₂C@NC) based on giant POM clusters of ((NH₄)₄₂[Mo₁₃₂O₃₇₂(CH₃COO)₃₀(H₂O)₇₂].₁₀CH₃COONH₄·300H₂O) (Mo₁₃₂) and tested its activity towards HER electrocatalysis in basic and acid media (1 M KOH and 0.5 M H₂SO₄). The material had an overpotential of 107 and 125 mV at 10 mA/cm² and a Tafel slope of 88 and 117 mV/dec, outperforming its monometallic counterparts and performing similarly to Pt/C benchmark electrocatalyst. The durability and stability properties were similar in acidic and alkaline conditions, with only a slight current drop after 48 h of operation and no structural or morphological changes after HER stability tests. The

TABLE 11 HER electrocatalysts and their key performance indicators: transition MOFs.

Electrocatalyst	η_{10} (mV)	Tafel slope (mV/dec)	Electrolyte	Source
MOF(Ni)-GR(4%)	268	108	1 M KOH	Dao et al. (2022)
Ni-MOF-800	356	127.3	0.5 M H ₂ SO ₄	Wu et al. (2022)
CoMnP/NF	66.6	38.8	0.5 M H ₂ SO ₄	Duan et al. (2022)
CoMnP/NF	53.9	63	1 M NaOH	Duan et al. (2022)
CoP/Co-MOF/CF	27	43	0.5 M H ₂ SO ₄	Liu et al. (2019)
CoP/Co-MOF/CF	34	56	pH 7 PBS ^a buffer	Liu et al. (2019)
CoP/Co-MOF/CF	49	63	1 M KOH	Liu et al. (2019)
Co-MOF-800	193	77.1	0.5 M H ₂ SO ₄	Pan et al. (2019)
Meso-Cu-BTC MOF	-	33.41	1 M NaOH	Nivetha et al. (2020)
rhombic octahedral Cu-BTC	53	62	0.5 M H ₂ SO ₄	Zhang et al. (2020)
rod-shaped Co-BTC	123	100	0.5 M H ₂ SO ₄	Zhang et al. (2020)
spherical Ni-BTC	270	155	0.5 M H ₂ SO ₄	Zhang et al. (2020)

a) PBS, phosphate buffer solution.

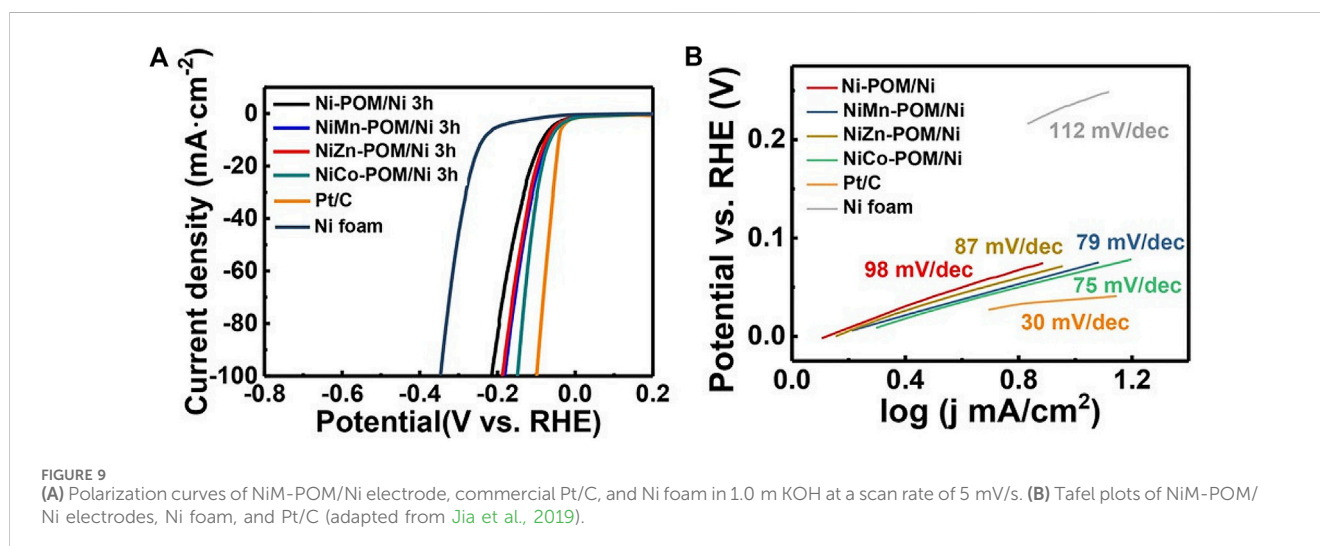


FIGURE 9

(A) Polarization curves of NiM-POM/Ni electrode, commercial Pt/C, and Ni foam in 1.0 M KOH at a scan rate of 5 mV/s. (B) Tafel plots of NiM-POM/Ni electrodes, Ni foam, and Pt/C (adapted from Jia et al., 2019).

performance was attributed to the improved electronic structure with nickel doping and the higher exposition of active sites due to the mesoporous structure (Sun et al., 2023).

Jia et al. reported the production of nickel foam-supported Dexter-Silverton-type bimetallic POMs NiM-POMs ($M = \text{Co}, \text{Zn}, \text{Mn}$) using Keggin POM clusters as building blocks and tested their catalytic activities towards HER in basic conditions (1 M KOH). The POMs HER polarization curves are presented in Figure 9. These materials exhibited overpotentials at 10 mA/cm² of 64, 68, 74, and 83 mV, and Tafel slopes of 75, 79, 87, and 98 mV/dec, respectively for NiCo-POM/Ni, NiMn-POM/Ni, NiZn-POM/Ni, and Ni-POM/Ni. The performance was correlated to the microcrystal size, with the range between 2–4 μm associated with the highest activity. The stability of NiCo-POM/Ni was also demonstrated, as no reasonable differences in performance or morphology were observed after 2,000 cycles. The good performance was attributed to the intrinsic reactivity of POM microcrystals with abundant active sites (Jia et al., 2019).

Zhang Z. et al. have designed Ni-modified PW₁₂ clusters with 3D nanoflower structure grown on Ni foam (NF) and tested its electrocatalytic potential towards HER in alkaline medium (1 M KOH). The study demonstrated that the overpotential needed to reach 10 mA/cm² was 75 mV and that the Tafel slope was 86 mV/dec, slightly underperforming the benchmark Pt/C electrocatalyst. Additionally, there was practically no activity loss after 2,000 cycles, being kept for at least 30 h with no morphological or structural changes. The activity was attributed to the synergistic effect between Ni and W, the electric conductivity of the NF support, and the enhanced number of exposed active sites due to the unique micro-nanostructure (Zhang et al., 2022).

Zhang Z. et al. synthesized a two-fold interpenetrating POMOF compound, [(Ni₃(bpp)₃(H₂O)₁₁(PW₉^{VI}W₃^{VO}₄₀)]·2H₂O (bpp = 3, 5'-bis(pyrid-4-yl)pyridine), and tested it for HER in basic electrolyte (1 M KOH). The produced electrocatalyst presented an overpotential of 74.6 mV to achieve 10 mA/cm² and a Tafel slope

of 111 mV/dec, slightly underperforming the benchmark Pt/C electrocatalyst, but demonstrating great stability properties due to no apparent decline in activity after 2,000 cycles and stable activity for more than 48 h. The activity was attributed to the synergistic effects between the enclosed POM and MOF complex and the highly exposed surface area (Zhang et al., 2023a).

Jawale et al. immobilized Ni-containing Dawson and sandwich-type POMs on the surface of carbon nanotubes and later tested their electrocatalytic properties towards HER in acid conditions (0.5 M H₂SO₄). It was verified that the Tafel slopes were in the 121–125 mV/dec range, but the catalysts still underperformed the Pt/C benchmark electrocatalyst. The enhanced performance was attributed to the number of Ni centers in the structure (a higher number of centers implied higher performance) and to the structure of the POM itself (the sandwich structure was able to contain a higher number of Ni centers) (Jawale et al., 2022).

Ahmad et al. immobilized a Mn sandwich POM, Na₁₀[Mn₄(H₂O)₂(VW₉O₃₄)₂].26H₂O, on the surface of CoSe₂ nanobelts (CoSe₂-NB) and tested its catalytic activity towards HER in acidic medium (0.5 M H₂SO₄). The composite attained a 187 mV overpotential at 10 mA/cm² and a Tafel slope of 55 mV/dec, with no difference in performance or morphology after 2,000 cycles and no noticeable current drop after 24 h of operation. The performance was attributed to the 3D structural framework, high conductivity and surface area of the support, and the synergistic effects in the microenvironment induced by decorating sandwich-type POMs on the surface of CoSe₂-NBs (Ahmad et al., 2020).

Xu et al. designed a cobalt and tungsten-based bimetallic electrocatalyst based on a bimetallic POM, [Co₉(OH)₃(H₂O)₆(HPO₄)₂(PW₉O₃₄)₃]¹⁶⁻ via a one-step calcination process, Co/WC@NC, and tested its properties toward HER electrocatalysis in acid and basic solutions (0.5 M H₂SO₄ and 1 M KOH). The results demonstrated that Co/WC@NC presented an overpotential of 129 and 142 mV to reach 10 mA/cm² and a Tafel slope of 93 and 91 mV/dec for acid and basic conditions, respectively, outperforming the catalyst's monometallic counterparts. Furthermore, the activity shows only a small decline after 2,000 cycles, with no significant decrease after 24 h of continuous operation in both solutions, and no morphological or structural changes. The activity was attributed to the synergistic interactions between the two metals, which regulate the electronic structure of the catalyst and enhance conductivity and activity, as well as the protective effect of the carbon layers, which prevents metal corrosion, and N-doping, contributing to a faster charge transfer (Xu et al., 2021).

Chen C. et al. disclosed the use of a POMOF-derived bi-transition metal carbide (Mo_xCo_xC) confined in uniform carbon polyhedrons synthesized via calcination after the formation of a POMOF-based on PMo₁₂ Keggin POM and ZIF-67 MOF as an HER electrocatalyst in basic conditions (1 M KOH). Regarding the cathodic water splitting reaction, the material, PMo/ZIF-67-6-6N, needed an overpotential of 83 mV to deliver 10 mA/cm² and had a Tafel slope of 50 mV/dec. Additionally, there was a negligible change in activity after 1,000 cycles, and the performance remained stable for 22 h. The activity was attributed to the small particle size of the formed carbides, which exposed more active sites, to the N-doped carbon coating that stabilized the carbides, the synergistic effects between the metals and the support structure, and the porous structure itself (Chen C. et al., 2018).

Wang et al. reported the synthesis of 2D CoMo-POMOF nanopillar arrays on a conductive Ni foam substrate and its electrocatalytic activity in acid medium (0.5 M H₂SO₄). The results demonstrated that it needed an overpotential of 137 mV to attain 10 mA/cm² and that it had a Tafel slope of 59 mV/dec, slightly underperforming the state-of-the-art Pt/C electrocatalyst. Additionally, good stability was verified, since the performance was practically unchanged and the morphological and structural characteristics were well maintained after 2,000 cycles. The activity was attributed to the self-supported open construction of nanopillar arrays, optimized Gibbs free energy of hydrogen adsorption, and the 2D nanosheets of CoMo-POMOF (Wang et al., 2022).

Shen et al. studied the HER performance of a new XC-72 carbon black supported Lindqvist POM-based inorganic-organic compound with a porous intercalation structure, [Cu₂(bimb)₂(ox)](W₆O₁₉)·4H₂O [bimb = 1,3-bis(1-imidazolyl) benzene, ox = oxalic acid] in acid conditions (0.5 M H₂SO₄). The material needed an overpotential of 146 mV to reach 10 mA/cm² and had a Tafel slope of 69 mV/dec, performing closely to benchmark Pt/C HER electrocatalyst. The performance was attributed to the higher electronic conductivity of the carbon black support, hexatungstate fragments originating from the Lindqvist structure that act as active sites, and the porous intercalation structure present in the material (Shen et al., 2019).

Zang et al. disclosed the synthesis of Anderson-type POM-modified Cu nanomaterials on TiO₂ nanotube array and tested their potential as HER electrocatalysts in acid medium (0.5 M H₂SO₄). The best composite material, NiMo₆O₂₄@Cu/TNA, presented a 215 mV overpotential to attain 10 mA/cm² and presented a Tafel slope of 89.2 mV. Furthermore, there was a negligible shift in performance after 500 cycles, and no apparent current decrease after 3 h of operation. The activity was attributed to the synergy between the utilized POMs and Cu to produce a dendrite morphology that exposed more active surface area and modified the local electrochemical environment of the active sites, enhancing the HER (Zang et al., 2019).

Fernandes et al. prepared a series of nanocomposites based on three different POMs supported on reduced oxidized graphene flakes, P₂W₁₈@rGF_{ox}, P₅W₃₀@rGF_{ox}, and P₈W₄₈@rGF_{ox}, and tested their HER electrocatalytic properties in acid medium (0.5 M H₂SO₄). The materials showed an overpotential for 10 mA/cm² of 35, 33, and 44 mV, and a Tafel slope of 37, 33, and 41, for P₂W₁₈@rGF_{ox}, P₅W₃₀@rGF_{ox}, and P₈W₄₈@rGF_{ox}, respectively, with performances that closely resembled that of benchmark Pt/C electrocatalyst. However, stability tests were only made for P₅W₃₀@rGF_{ox} and showed no significant changes after 1,000 cycles. The activity was attributed to the well-known POM property of undergoing reversible multi-electron reduction/oxidation without structural changes and the high electronic conductivity and porous network of the support, enhancing charge transfer rate and catalyst loading capabilities (Fernandes et al., 2018b).

Table 12 contains the HER key performance indicators for the analyzed POM-based electrocatalysts.

5 Bifunctional materials for OER/ORR

Wu et al. produced mesoporous NiO and NiCo₂O₄ using a hydrothermal template-free synthesis and tested them as

TABLE 12 HER electrocatalysts and their key performance indicators: transition metal POMs.

Electrocatalyst	η_{10} (mV)	Tafel slope (mV/dec)	Electrolyte	Source
Ni/Mo ₂ C@NC	107	88	1 M KOH	Sun et al. (2023)
Ni/Mo ₂ C@NC	125	117	0.5 M H ₂ SO ₄	Sun et al. (2023)
NiCo-POM/Ni	64	75	1 M KOH	Jia et al. (2019)
NiMn-POM/Ni	68	79	1 M KOH	Jia et al. (2019)
NiZn-POM/Ni	74	87	1 M KOH	Jia et al. (2019)
Ni-POM/Ni	83	98	1 M KOH	Jia et al. (2019)
Ni-WO/NF	75	86	1 M KOH	Zhang et al. (2022a)
Ni ₃ W ₉ V ₁ W ₃ ^V	74.6	111	1 M KOH	Zhang Z. et al. (2023a)
Mn ₄ V/CoSe ₂	187	55	0.5 M H ₂ SO ₄	Ahmad et al. (2020)
Co/WC@NC	129	93	0.5 M H ₂ SO ₄	Xu et al. (2021)
Co/WC@NC	142	91	1 M KOH	Xu et al. (2021)
CoMo-POMOF nanopillar arrays	137	59	0.5 M H ₂ SO ₄	Wang et al. (2022)
PMo/ZIF-67-6-6N	83	50	1 M KOH	Chen et al. (2018)
Cu ₂ W ₆	146	69	0.5 M H ₂ SO ₄	Shen et al. (2019)
NiMo ₆ O ₂₄ @Cu/TNA	215	89.2	0.5 M H ₂ SO ₄	Zang et al. (2019)
P ₂ W ₁₈ @rGF_ox	35	37	0.5 M H ₂ SO ₄	Fernandes et al. (2018b)
P ₅ W ₃₀ @rGF_ox	33	33	0.5 M H ₂ SO ₄	Fernandes et al. (2018b)
P ₈ W ₄₈ @rGF_ox	44	41	0.5 M H ₂ SO ₄	Fernandes et al. (2018b)

bifunctional catalysts for the OER/ORR reactions pair in alkaline medium (0.1 M KOH). Concerning the OER, NiCo₂O₄ showed a lower Tafel slope, indicating better kinetics towards this reaction. NiCo₂O₄ also showed a better performance towards the ORR, which is confirmed by a higher onset potential and higher number of exchanged electrons, demonstrating higher selectivity towards the 4e⁻ reduction pathway. This is further corroborated by the lower observed local yield of H₂O₂, 20% for NiO, against 5% for NiCo₂O₄. Additionally, NiCo₂O₄ showed good stability properties, with only ~50 mV potential loss during 50 h of operation. The exhibited performance was attributed to the higher number of surface hydroxyl adsorbates that can promote the 4e⁻ ORR path in NiCo₂O₄, as well as the synergistic effects of having a bimetallic Co and Ni oxide composition ([Wu et al., 2023](#)).

In a more innovative fashion, Sivakumar et al. tested three ternary Ni-Co-Mn oxides as bifunctional catalysts for OER/ORR in alkaline medium (0.1 M KOH), NiCoMnO₄, Ni_{1.5}Co_{0.75}Mn_{0.75}O₄ and Ni₂Co_{0.5}Mn_{0.5}O₄. They all presented good stability, and the best-performing material, Ni_{1.5}Co_{0.75}Mn_{0.75}O₄, showed similar behavior to IrO₂ for OER. Although its ORR activity was still far behind Pt/C, its bifunctional activity was higher than both IrO₂ and Pt/C ([Sivakumar et al., 2019](#)).

Xing et al. tested OER/ORR bifunctionality of two nanoparticulate manganese vanadium oxide deposited on a nitrogen-doped reduced graphene oxide in alkaline medium (0.1 M KOH). The samples differed in the total time they were subjected to a thermal treatment. The OER study showed that the composites had good stability under the reaction conditions and

good electrocatalytic performance, as they could achieve a 10 mA/cm² current density at overpotentials of 440 and 420 mV. However, the materials had a Tafel slope of 286 and 271 mV/dec, indicating that there is still much room for improvement in terms of OER performance. For the ORR, both electrocatalysts demonstrated a 4e⁻ pathway and stability over at least a 4-h period, as well as superior activity when compared to the benchmark Pt/C electrocatalyst ([Xing et al., 2018](#)).

Belkessam et al. synthesized spinel structure Ni and Co mixed metal transition oxides by using a facile sol-gel method with different metal salt precursors, namely, their chlorides (Cl-NiCoO), sulfates (S-NiCoO), and nitrates (N-NiCoO), and tested their activity for OER and ORR in alkaline conditions (0.1M KOH). Regarding the OER, the best-performing electrocatalyst was S-NiCoO. This was linked to the presence of Ni³⁺ as the main oxidation state for Ni and to the presence of sulfide, which increased the number of active sites and the coordination of Ni/Co. Relative to the ORR, the results showed Cl-NiCoO had the highest activity, albeit its selectivity to the 2e⁻ pathway. These different activities were attributed to the different morphologies obtained for each sample and to the presence of the precursor anion, which could act as a doping element ([Belkessam et al., 2020](#)).

Wang et al. designed iron, nickel, and nitrogen-doped carbon nanofibers (Fe/Ni-N-CNFs) via an electrospinning technique and tested their activities for the OER/ORR pair in alkaline conditions (0.1 M KOH). The best-performing composite, with a 1:1 Fe to Ni ratio, performed better than the mono-metallic composites and compared itself to the benchmark Pt/C electrocatalyst,

exchanging an average of 3.97 electrons during the reduction process. This electrocatalyst also demonstrated the best OER performance, with the lowest Tafel slope and higher currents for the tested OER polarization region, and it was determined to have the best bifunctional characteristics towards those reactions. The electrocatalyst also demonstrated stability after 2,000 CV cycles, and its performance was attributed to the metal alloying synergistic interactions, N doping, structural defects, and the 3D porous cross-linked microstructure (Wang et al., 2017).

Abdelkader-Fernández et al. reported the synthesis of noble-metal-free dual N,S-doped MOF-74-derived nanostructured carbon-based materials, outlining the effects of the type of doping and the metal composition in the MOF-74 template in the OER and ORR performances in 0.1 M KOH. They found that, individually, N,S-dual-doping (mainly in the Co-based MOF-74) and the use of two metals (Ni and Co) in the MOF-74 template structure were able to enhance the OER activities, making them comparable to state-of-the-art IrO₂ and other similar reported materials. However, they demonstrated an adverse effect when used simultaneously. This was explained by the fact that the bimetallic dual-doped sample involves Co_xNi_{1-x}S sulfide instead of CoS, present in the purely dual-doped sample and more active for OER, and that it does not show “active” core/shell nanostructures, unlike the purely bimetallic sample. For the ORR, the dual-doping strategy increased the exhibited performances, albeit in a more limited manner, while the metal composition showed no significant effect on performance (Abdelkader-Fernández et al., 2019).

Yusinova et al. performed the pyrolysis of a mixed metal Mn/Co MOF (TAL-42) to produce an electrocatalyst active towards ORR and OER in alkaline medium (0.1 M KOH). The best-performing composite material towards ORR, TAL-42-900, presented an activity comparable to Pt/C, and superior stability properties. TAL-42-900 also exhibited the lowest overpotentials and Tafel slopes for the OER, performing better than the RuO₂ benchmark electrocatalyst and being classified as the best bifunctional material amongst the tested electrocatalysts. The activity was attributed to the mesoporous structure, large surface area, and the presence of M-N_x species (M = Mn,Co) (Yusibova et al., 2023).

Wahab et al. reported the use of Mn-MOF@rGO nanocomposite as a bifunctional catalyst for both ORR and OER in alkaline conditions (0.1 M KOH and 1 M KOH, respectively). Regarding the ORR, the best-performing sample, MnBDC@75%rGO, compared itself to the benchmark Pt/C electrocatalyst and presented good methanol crossover resistance. Relatively to the OER, the electrocatalyst demonstrated better activity than Pt/C, with a 610 mV overpotential to achieve 10 mA/cm² and a Tafel slope of 83 mV/dec. The good performance was attributed to the synergistic effects between the mesoporous 3D framework and the transition metal-organic composition (Wahab et al., 2020).

Zhang M.-C. et al. synthesized a bimetallic CuCo MOF to work as a bifunctional electrocatalyst for OER/ORR in alkaline (0.1 M KOH) and neutral media. Regarding the alkaline OER, the material needed a 400 mV overpotential to achieve 10 mA/cm² and had a Tafel slope of 122.3 mV/dec with good current retention properties. Regarding the neutral OER, the overpotential needed to reach 10 mA/cm² was 550 mV, and the obtained Tafel slope was 276.1 mV/dec, also with good retention properties. In both cases,

the bimetallic MOF had better performance than the monometallic Cu MOF. The ORR performance followed the same trend: the bimetallic MOF performed better than the monometallic Cu MOF, and the performance of both materials was higher in alkaline conditions, with the bimetallic MOF being ultimately considered the best bifunctional material. The higher activity was attributed to a higher exposition of active sites and the synergistic effect of the bimetallic active sites, which increased charge transfer efficiency at the catalyst electrode/electrolyte interface (Zhang et al., 2023c).

Lu et al. reported the synthesis of metallic Co nanoparticles embedded in N-doped porous carbon layers (Co@NPC-T, T = 800, 900, or 1,000°C), using macroscale Co-MOF crystals as a precursor, and its use as a bifunctional electrocatalyst for ORR and OER in alkaline medium (0.1 M KOH). For the OER, the best-performing material, Co@NPC-900, needed 380 mV of overpotential to achieve 10 mA/cm² and presented good stability properties. Regarding the ORR, the activity was comparable to that of benchmark Pt/C with higher stability properties, and it was determined that Co@NPC-900 and Co@NPC-1,000 have similar bifunctional characteristics that are superior to those of Co@NPC-800. The verified performance was attributed to the improved electron transfer due to the graphitic carbon structure and to the synergistic effects between the metal and the graphitic carbon structure (Lu et al., 2017).

Marques et al. assembled sandwich-type Dawson family POMs anchored in N-doped multi-walled carbon nanotubes (MWCNT_N6) and tested their electrocatalytic properties towards OER and ORR in alkaline medium (0.1 M KOH). Regarding the OER, the three POMS@MWCNT_N6 (Ni₄, Fe₄, and Ni₂Fe₂) composites presented overpotentials of 580, 460, and 360 mV to achieve 10 mA/cm² and Tafel slopes of 102, 54, and 45 mV/dec for Fe₄@MWCNT_N6, Ni₄@MWCNT_N6, and Ni₂Fe₂@MWCNT_N6, respectively. Furthermore, tests at 500 mV of overpotential for 12 h showed that Fe₄ and Ni₄ retained 80% and 87% of their current and Fe₂Ni₂ retained 64%, indicating that the bimetallic Fe-Ni composite had the worst stability properties, even though it was the best-performing material. Relative to the ORR, the results indicate that an onset potential of ~0.8 V vs RHE was obtained for all materials, and Tafel slopes of 35.4, 34.7, and 37.9 mV/dec were obtained for Fe₄, Ni₄, and Fe₂Ni₂, respectively. Lastly, the number of transferred electrons is around 3, thus suggesting a mixed regime between the 4 and 2 electrons pathway, and good stability for the Fe₄ and Ni₂Fe₂ (84% and 80% of current retention after 12 h) was observed at ORR conditions (Marques et al., 2022).

Limani et al. prepared a series of Co-POMs anchored on doped carbon materials (MWCNT_N8_Co4, GF_N8_Co4, GF_ND8_Co4, and GF_NS8_Co4) and tested their performance for ORR and OER at alkaline conditions (0.1 M KOH). The ORR results demonstrated that the best-performing material (MWCNT_N8_Co4) had a performance comparable to that of benchmark Pt/C and good stability properties, along with high methanol crossover tolerance, indicating its durability. Relative to the OER results, the catalysts demonstrated activities that very closely resembled those of benchmark IrO₂ and RuO₂ electrocatalysts, with the best-performing material, GF_N8_Co4, outperforming IrO₂ and showing relatively good stability after almost 10 h of operation. No metric was calculated to determine the best bifunctional

TABLE 13 MOF and POM(-derived) bifunctional OER/ORR electrocatalysts.

Electrocatalyst	OER η_{10} (mV)	OER Tafel slope (mV/dec)	ORR Tafel slope (mV/dec)	ΔE^b (V)	Electrolyte	Source
NiCo ₂ O ₄	340	50	-	-	0.1 M KOH	Wu et al. (2023)
NiO	380	56	-	-	0.1 M KOH	Wu et al. (2023)
Ni _{1.5} Co _{0.75} Mn _{0.75} O ₄	570	68	-	0.79	0.1 M KOH	Sivakumar et al. (2019)
MnVOx@N-rGO-440	440	286	66.6	-	0.1 M KOH	Xing et al. (2018)
MnVO _x @N-rGO-900	420	271	130.9	0.85	0.1 M KOH	Xing et al. (2018)
N-NiCoO	-	-	-	-	0.1 M KOH	Belkessam et al. (2020)
S-NiCoO	340	-	-	-	0.1 M KOH	Belkessam et al. (2020)
Cl-NiCoO	-	-	-	-	0.1 M KOH	Belkessam et al. (2020)
Fe/Ni-N-CNFs	372	106.1	61.2	0.80	0.1 M KOH	Wang et al. (2017)
TAL-42-900	410	71	45	0.80	0.1 M KOH	Yusibova et al. (2023)
MnBDC@75%rGO	610	83	93.5	-	1 M KOH	Wahab et al. (2020)
CuCo-HITP	400	122.3	96.4	0.94	0.1 M KOH	Zhang M.-C. et al., 2023
CuCo-HITP	550	276.1	319.3	1.41	0.1 M PBS ^a	Zhang M.-C. et al., 2023
Co@NPC-900	380	-	-	0.85	0.1 M KOH	Lu et al. (2017)
Ni ₄ @MWCNT_N6	580@0.1 mA/cm ²	102	34.7	-	0.1 M KOH	Marques et al. (2022)
Fe ₄ @MWCNT_N6	460@0.1 mA/cm ²	54	35.4	-	0.1 M KOH	Marques et al. (2022)
Ni ₂ Fe ₂ @MWCNT_N6	360@0.1 mA/cm ²	45	37.9	-	0.1 M KOH	Marques et al. (2022)
MWCNT_N8_Co4	400	55	41	-	0.1 M KOH	Limani et al. (2022)
GF_N8_Co4	340	67	50	-	0.1 M KOH	Limani et al. (2022)
GF_ND8_Co4	490	68	90	-	0.1 M KOH	Limani et al. (2022)
GF_NS8_Co4	460	62	40	-	0.1 M KOH	Limani et al. (2022)

a) PBS, phosphate buffer solution.

b) ΔE , means the difference between the ORR, half-wave potential and the OER, potential to attain 10 mA/cm². Lower values indicate a better material in terms of bifunctionality. The ORR, potential to achieve 3 mA/cm² may be used instead of the half-wave potential.

electrocatalyst, but all the tested materials presented bifunctionality towards those two reactions (Limani et al., 2022).

Table 13 groups the aforementioned bifunctional OER/ORR electrocatalysts and their performance parameters.

6 Bifunctional materials for OER/HER

Zhou et al. described the use of trimetallic MOF-74 (Mn_xFe_yNi-MOF-74) films grown on nickel foam as bifunctional electrocatalysts for OER and HER in alkaline medium (1 M KOH). The OER activity of the optimized film, Mn_{0.52}Fe_{0.71}Ni-MOF-74, surpassed its bimetallic counterparts, Mn_{2.67}Ni-MOF-74 and Fe_{1.88}Ni-MOF-74, as well as the state-of-the-art IrO₂ electrocatalyst. HER activity of the same optimized film was superior to its bimetallic counterparts and comparable to the benchmark Pt/C electrocatalyst, and the film showed good stability in both OER and HER polarization conditions. The enhanced performance was attributed to Mn doping, which exposed more active sites, regulated charge transfer, and formed oxyhydroxides, acting as active phases in the electrocatalyst. Finally, a 2-electrode water electrolyzer (1 M KOH) with the optimized film as both cathode and anode was built

to test the material's overall water splitting capabilities, with 10 mA/cm² being achieved at a 1.48 V and overall stability for over 100 h at 200 mA/cm² being observed (Zhou et al., 2020).

Chen et al. reported the synthesis of a carbon-coated Co-doped selenide nanomaterial derived from nickel-cobalt bimetallic MOF, NiCoSe/C, and tested it as an overall water splitting electrocatalyst in alkaline medium (1 M KOH). The OER tests demonstrated a superior performance, with a low overpotential of 249 mV at 10 mA/cm², and good stability properties, outperforming the benchmark RuO₂ electrocatalyst. HER results, albeit not superior to benchmark Pt/C, were still significantly lower than other NiCo-based materials, with the material presenting excellent stability properties. Finally, a two-electrode cell was constructed to verify the overall water-splitting activity, with NiCoSe/C acting as both cathode and anode. The resulting cell was able to deliver 10 mA/cm² at 1.68 V and showed stability both for over 20 h of operation and after 1,000 operation cycles. The performance was attributed to the synergy between Ni and Co, which modulated the material's electronic structure, and to the highly porous and high specific surface area structure inherited from the parent MOF (Chen Z. et al., 2019).

Zhao et al. prepared Mo-CoS₂ nanoparticles embedded in a hierarchically porous carbon hollow sphere, Mo-CoS₂/NC (H),

derived from ZIF-67 MOF, phosphomolybdic acid POM and polystyrene sphere. The resulting composite was tested as an overall water-splitting electrocatalyst in 1 M KOH. The OER results demonstrated that the produced nanoparticles outperformed the benchmark RuO₂ electrocatalyst and exhibited good stability properties. Regarding HER, the material presented activity comparable to that of state-of-the-art Pt/C, alongside good stability. Regarding the overall water splitting activity, an electrolyzer where Mo-CoS₂/NC (H) acted as both cathode and anode was constructed, and it delivered 10 mA/cm² at 1.59 V vs RHE, which is comparable to other state-of-the-art water splitting catalysts. The enhanced activity was attributed to strengthened chemical adsorption of H and O, higher electrical conductivity due to Mo incorporation, and the micro/meso/macro porous structure, which offers a large specific surface area and a high number of active sites (Zhao et al., 2023).

Zhao et al. disclosed the use of a Ni-Fe bimetallic MOF-derived electrocatalyst, Fe-Ni@NC-CNTs, as an overall water-splitting electrocatalyst in alkaline solution (1 M KOH). The OER results indicated a good overall activity, with a 274 mV overpotential at 10 mA/cm² and a 45.5 mV/dec Tafel slope. Relative to the HER, the tested material exhibited a performance comparable to that of benchmark Pt/C, and also demonstrated good stability properties at HER and OER polarization conditions. The performance of Fe-Ni@NC-CNTs as an overall water-splitting electrocatalyst was tested in an electrolyzer where it acts both as the cathode and as the anode, attaining a 145 mA/cm² current density at 1.98 V vs RHE, which is comparable to the performance of an electrolyzer containing Pt/C as the cathode and Ir/C as the anode. The observed performance was attributed to the high conductivity and hierarchical pore structure, which resulted in both high activity and fast mass transport (Zhao et al., 2018).

Gao et al. deposited a mixed Cu, Co, and W metal oxide nanostructure onto a copper foam electrode by using [SiW₁₁O₃₉]⁸⁻-POM as a structure directing agent and tested its performance towards OER and HER in alkaline conditions (0.1 M KOH). Regarding the OER, the obtained electrocatalyst needed an overpotential of 313 mV to reach a current density of 10 mA/cm². The HER results show that a 103 mV overpotential was needed to achieve 10 mA/cm² and the material presented stability for over 10 h in both HER and OER polarization conditions. The material was also tested as an overall water-splitting bifunctional material in a 2-electrode water electrolyzer

(0.1 M KOH electrolyte), with sustained gas evolution being observed at 1.8 V vs RHE (Gao et al., 2019).

Zhang Z. et al. derived CoMoO₄ hollow tubes (HT) from the annealing of a PMo₁₂@Co-BTC POMOF hybrid and tested its ability to act as an overall water-splitting electrocatalyst in 1 M KOH. The OER activity proved superior to benchmark RuO₂, and the material exhibited excellent stability properties. The HER activity was comparable to state-of-the-art Pt/C but did not surpass it, and CoMoO₄ HTs also demonstrated excellent stability properties. Finally, a two-electrode cell with the CoMoO₄ HTs acting as both cathode and anode was constructed to test the overall water-splitting capabilities and was compared to a similar cell constructed with Pt/C as the cathode and RuO₂ as the anode. The results indicated that a current density of 10 mA/cm² was attained at 1.57 V vs RHE for the first cell and 1.50 V vs RHE for the second cell, demonstrating that the material presented impressive overall water-splitting capabilities. The superior performance was attributed to the presence of a hollow and rough surface, which increased specific surface area, the mesoporous structure, which increased mass-transfer and charge-transfer rates due to more access points, and the inherent conductivity of Co-based materials (Zhang Z. et al., 2023b).

Gautam et al. designed a POM-anchored zinc cobalt sulfide nanowires on 3D Ni foam substrate (POM@ZnCoS/NF, POM = PW₁₂) to be used as an overall water splitting electrocatalyst in alkaline electrolyte (1 M KOH). The material presented better OER activity than benchmark RuO₂, and also had good stability properties, maintaining activity for over 20 h without structural changes. It also presented impressive HER activity, surpassing even benchmark Pt/C, and good stability, being able to consistently demonstrate activity for over 20 h without structural changes. A 2-electrode water splitting cell using POM@ZnCoS/NF as both cathode and anode was tested: it delivered 10 mA/cm² at 1.55 V vs RHE, outperforming a similar cell that used Pt/C as cathode and RuO₂ as anode (1.64 V vs RHE at 10 mA/cm²). The observed performance was attributed mainly to the mesoporous hierarchical heterostructure, which improved the conductivity and increased both the number of available active sites and the electrochemical surface area (Gautam et al., 2021). The discussed bifunctional materials for OER/HER are summarized in Table 14, along with the relevant performance indicators.

TABLE 14 MOF and POM(-derived) bifunctional OER/HER electrocatalysts.

Electrocatalyst	OER η_{10} (mV)	OER Tafel slope (mV/dec)	HER η_{10} (mV)	HER Tafel slope (mV/dec)	Electrolyte	Source
Mn _{0.52} Fe _{0.71} Ni-MOF-74	267@100 mA/cm ²	36.7	190@100 mA/cm ²	103.8	1 M KOH	Zhou et al. (2020)
NiCoSe/C	249	54	143	104.8	1 M KOH	Chen Z. et al. (2019)
Mo-CoS ₂ /NC (H)	296	65	158	150	1 M KOH	Zhao et al. (2023)
Fe-Ni@NC-CNTs	274	45.5	202	113.7	1 M KOH	Zhao et al. (2018)
CuCoWO _x	313	162	103	335	0.1 M KOH	Gao et al. (2019)
CoMoO ₄ HTs	210	80.3	75	89.1	1 M KOH	Zhang et al. (2023b)
POM@ZnCoS NWs	200@20 mA/cm ²	67.7	170	53.5	1 M KOH	Gautam et al. (2021)

The future perspective of transition metal-based catalysts as a whole is one of optimism. There are dozens of studies highlighting the advantages of combining those abundant metals to replace current state-of-the-art noble metals in electrochemical energy conversion and storage, be it in the form of the more traditional oxide and alloy catalysts or in the form of the more modern POM and MOF catalysts (and their derivatives). Additionally, the versatility of transition metal catalysts is not limited to those four material classes, as other transition metal-based materials are also reviewed herein, including carbides, phosphides, and nitrides, which can also be derived from POMs and MOFs. Finally, the high tunability and structural versatility of POMs and MOFs means that there are multiple combinations to be applied in electrocatalyst materials, each with its own catalytic prowess, and some of them are yet to be studied. As such, this review's main scope was to analyze some of those combinations for those two classes and compare them to the traditional electrocatalyst classes to bring a comprehensive understanding of the real catalytic capabilities of POMs and MOFs.

7 Conclusion

The electrochemical reactions involved in the main energy conversion and storage systems, OER, ORR, and HER, are sluggish, and their electrocatalysts are expensive since they are based on scarce noble metals. As alternatives to these benchmark electrocatalysts, transition metal-based POM and MOF-derived electrocatalysts are being studied. Their main advantage resides in the tailorability these structures present, meaning that one can easily modify it in the desired manner, normally through simple adaptations in the synthetic process. This means that when one of those materials is faced with performance or stability issues, they can be easily adapted, for example, by adding moieties that can enhance these aspects, thus generating a better-performing material. Additional strategies include inducing the formation of a core-shell nanostructure, where the active material in the core is protected by the external shell, enhancing stability, and anchoring POMs or MOFs on conductive supports, which can both enhance the activity and stability of the utilized materials. Their performance is comparable to that of the more traditional

transition metal-based oxide and alloy electrocatalysts, meaning they show a promising future in the electrocatalysis application.

Author contributions

HA: Investigation, Validation, Writing—original draft. BS: Conceptualization, Funding acquisition, Project administration, Writing—review and editing. SG: Conceptualization, Resources, Supervision, Writing—review and editing. DS: Conceptualization, Project administration, Resources, Supervision, Writing—review and editing.

Funding

The author(s) declare that no financial support was received for the research, authorship, and/or publication of this article. The authors would like to thank Fundação para a Ciência e a Tecnologia (FCT, Portugal) for funding EXPL/EQU-EQU/0517/2021 project, contract IST-ID/156/2018 (BŠ), and a contract in the scope of programmatic funding UIDP/04540/2020 (D.M.F. Santos), and projects LA/P/0008/2020 DOI 10.54499/LA/P/0008/2020, UIDP/50006/2020 DOI 10.54499/UIDP/50006/2020 and UIDB/50006/2020 DOI 10.54499/UIDB/50006/2020), through national funds.

Conflict of interest

The authors declare that the research was conducted in the absence of any commercial or financial relationships that could be construed as a potential conflict of interest.

Publisher's note

All claims expressed in this article are solely those of the authors and do not necessarily represent those of their affiliated organizations, or those of the publisher, the editors and the reviewers. Any product that may be evaluated in this article, or claim that may be made by its manufacturer, is not guaranteed or endorsed by the publisher.

References

- Abdelkader-Fernández, V. K., Fernandes, D. M., Balula, S. S., Cunha-Silva, L., and Freire, C. (2020). Oxygen evolution reaction electrocatalytic improvement in POM@ZIF nanocomposites: a bidirectional synergistic effect. *ACS Appl. Energy Mat.* 3, 2925–2934. doi:10.1021/acsaem.0c00009
- Abdelkader-Fernández, V. K., Fernandes, D. M., Balula, S. S., Cunha-Silva, L., Pérez-Mendoza, M. J., López-Garzon, F. J., et al. (2019). Noble-metal-free MOF-74-derived nanocarbons: insights on metal composition and doping effects on the electrocatalytic activity toward oxygen reactions. *ACS Appl. Energy Mat.* 2, 1854–1867. doi:10.1021/acsaem.8b02010
- Ahmad, W., Gao, Q., Zhang, X.-L., Tan, W., Zhang, L., Gao, M.-R., et al. (2020). Sandwich-type polyoxometalate mediates cobalt diselenide for hydrogen evolution in acidic electrolyte. *Chem. Nano. Mat.* 6, 1164–1168. doi:10.1002/cnma.202,000106
- Al-Oweini, R., Sartorel, A., Bassil, B. S., Mirco, N., Berardi, S., Scandola, F., et al. (2014). Photocatalytic water oxidation by a mixed-valent MnIII₂MnIVO₃ manganese oxo core that mimics the natural oxygen-evolving center. *Angew. Chem. Int. Ed. Engl.* 53, 11182–11185. doi:10.1002/anie.201404664
- Amin, M., Shah, H. H., Fareed, A. G., Khan, W. U., Chung, E., Zia, A., et al. (2022). Hydrogen production through renewable and non-renewable energy processes and their impact on climate change. *Int. J. Hydrogen Energy* 47, 33112–33134. doi:10.1016/j.ijhydene.2022.07.172
- Ammam, M., Keita, B., Nadjo, L., Mbomekalle, I.-M., Ritorto, M. D., Anderson, T. M., et al. (2011). Cyclic voltammetry study of the Mn-substituted polyoxoanions [MnII₄(H₂O)₂(H₄AsW₁₅O₅₆)₂]¹⁸⁻ and [(Mn^{III}OH₂)Mn^{II}₂PW₉O₃₄]₂(PW₆O₂₆)]¹⁷⁻: electrodeposition of manganese oxides electrocatalysts for dioxygen reduction. *Electroanalysis* 23, 1427–1434. doi:10.1002/elan.201,000735
- Arcos, J. M. M., and Santos, D. M. F. (2023). The hydrogen color spectrum: techno-economic analysis of the available technologies for hydrogen production. *Gases* 3, 25–46. doi:10.3390/gases301,0002
- Bai, L., Wen, X., and Guan, J. (2019). Amorphous Fe Co Ni oxide for oxygen evolution reaction. *Mater. Today Energy* 12, 311–317. doi:10.1016/j.mtener.2019.02.004
- Bai, X., Wang, Q., and Guan, J. (2021). "Bimetallic Iron–Cobalt nanoparticles coated with amorphous carbon for oxygen evolution. *ACS Appl. Nano Mat.* 4, 12663–12671. doi:10.1021/acsnm.1c03208

- Belkessam, C., Bencherif, S., Mechouet, M., Idiri, N., and Ghilane, J. (2020). The effect of heteroatom doping on nickel cobalt oxide electrocatalysts for oxygen evolution and reduction reactions. *ChemPlusChem* 85, 1710–1718. doi:10.1002/cplu.2020.000436
- Bhuvanendran, N., Ravichandran, S., Kandasamy, S., Zhang, W., Xu, Q., Khotseng, L., et al. (2021). Spindle-shaped CeO₂/biochar carbon with oxygen vacancy as an effective and highly durable electrocatalyst for oxygen reduction reaction. *Int. J. Hydrogen Energy* 46, 2128–2142. doi:10.1016/j.ijhydene.2020.10.115
- Butt, F. A., Anwar, M., and Unal, U. (2021). Synthesis of metallic copper nanowires using dielectric barrier discharge plasma and their application in hydrogen evolution reaction. *Int. J. Hydrogen Energy* 46, 18866–18877. doi:10.1016/j.ijhydene.2021.03.020
- Cao, J., Li, H., Pu, J., Zeng, S., Liu, L., Zhang, L., et al. (2019). Hierarchical NiMo alloy microtubes on nickel foam as an efficient electrocatalyst for hydrogen evolution reaction. *Int. J. Hydrogen Energy* 44, 24712–24718. doi:10.1016/j.ijhydene.2019.07.229
- Chatenet, M., Pollet, B. G., Dekel, D. R., Dionigi, F., Deseure, J., Millet, P., et al. (2022). Water electrolysis: from textbook knowledge to the latest scientific strategies and industrial developments. *Chem. Soc. Rev.* 51, 4583–4762. doi:10.1039/D0CS01079K
- Chen, C., Wu, A., Yan, H., Xiao, Y., Tian, C., and Fu, H. (2018). Trapping [PMo₁₂O₄₀]³⁺ clusters into pre-synthesized ZIF-67 toward Mo_xCo_xC particles confined in uniform carbon polyhedrons for efficient overall water splitting. *Chem. Sci.* 9, 4746–4755. doi:10.1039/C8SC01454J
- Chen, Z., Xu, B., Yang, X., Zhang, H., and Li, C. (2019). Bimetallic metal-organic framework derived electrocatalyst for efficient overall water splitting. *Int. J. Hydrogen Energy* 44, 5983–5989. doi:10.1016/j.ijhydene.2019.01.082
- Cheng, W., Wu, Z.-P., Luan, D., Zang, S.-Q., and Lou, X. W. (2021). Synergetic cobalt-copper-based bimetal-organic framework nanoboxes toward efficient electrochemical oxygen evolution. *Angew. Chem. Int. Ed.* 60, 26397–26402. doi:10.1002/anie.202112775
- Chu, M., Wang, L., Li, X., Hou, M., Li, N., Dong, Y., et al. (2018). Carbon coated nickel-nickel oxide composites as a highly efficient catalyst for hydrogen evolution reaction in acid medium. *Electrochim. Acta* 264, 284–291. doi:10.1016/j.electacta.2018.01.140
- Cui, Z., Wang, S., Zhang, Y., and Cao, M. (2014). Engineering hybrid between nickel oxide and nickel cobaltate to achieve exceptionally high activity for oxygen reduction reaction. *J. Power Sources* 272, 808–815. doi:10.1016/j.jpowsour.2014.08.097
- Dai, W., Lu, T., and Pan, Y. (2019). Novel and promising electrocatalyst for oxygen evolution reaction based on MnFeCoNi high entropy alloy. *J. Power Sources* 430, 104–111. doi:10.1016/j.jpowsour.2019.05.030
- Dao, X., Nie, M., Sun, H., Dong, W., Xue, Z., Li, Q., et al. (2022). Electrochemical performance of metal-organic framework MOF(Ni) doped graphene. *Int. J. Hydrogen Energy* 47 (2022), 16741–16749. doi:10.1016/j.ijhydene.2022.03.176
- Draskovic, T. I., and Wu, Y. (2017). Electrocatalytic properties of cuprous delafossite oxides for the alkaline oxygen reduction reaction. *ChemCatChem* 9, 3837–3842. doi:10.1002/cctc.201700712
- Duan, D., Feng, J., Guo, D., Gao, J., Liu, S., Wang, Y., et al. (2022). MOF-derived cobalt manganese phosphide as highly efficient electrocatalysts for hydrogen evolution reaction. *Int. J. Hydrogen Energy* 47, 12927–12936. doi:10.1016/j.ijhydene.2022.02.037
- Feng, C., Li, Z., Wang, J., Yan, T., Dong, H., Feng, J., et al. (2019). Synthesis of metal-organic framework-derived cobalt disulfide with high-performance oxygen reduction reaction catalytic properties. *J. Electroanal. Chem.* 840, 27–34. doi:10.1016/j.jelechem.2019.03.056
- Fernandes, D. M., Araújo, M. P., Haider, A., Mougharbel, A. S., Fernandes, A. J. S., Kortz, U., et al. (2018b). Polyoxometalate-graphene electrocatalysts for the hydrogen evolution reaction. *Chemelectrochem* 5, 273–283. doi:10.1002/celc.201701210
- Fernandes, D. M., Novais, H. C., Bacsá, R., Serp, P., Bachiller-Baeza, B., Rodríguez-Ramos, I., et al. (2018a). Polyoxotungstate@Carbon nanocomposites as oxygen reduction reaction (ORR) electrocatalysts. *Langmuir* 34, 6376–6387. doi:10.1021/acs.langmuir.8b00299
- Flores-Lasluisa, J. X., Quilez-Bermejo, J., Ramirez-Pérez, A. C., Huerta, F., Cazorla-Amorós, D., and Morallón, E. (2019). Copper-doped cobalt spinel electrocatalysts supported on activated carbon for hydrogen evolution reaction. *Materials* 12, 1302. doi:10.3390/ma12081302
- Gao, D., Liu, R., Biskupek, J., Kaiser, U., Song, Y.-F., Streb, C., et al. (2019). Modular design of noble metal-free mixed metal oxide electrocatalysts for complete water splitting. *Angew. Chem. Int. Ed.* 58, 4644–4648. doi:10.1002/anie.201900428
- Gautam, J., Liu, Y., Gu, J., Ma, Z., Zha, J., Dahal, B., et al. (2021). Fabrication of polyoxometalate anchored zinc cobalt sulfide nanowires as a remarkable bifunctional electrocatalyst for overall water splitting. *Adv. Funct. Mat.* 31. doi:10.1002/adfm.202106147
- Ge, Y., Chen, J., Chu, H., Dong, P., Craig, S. R., Ajayan, P. M., et al. (2018). Urchin-like CoP with controlled manganese doping toward efficient hydrogen evolution reaction in both acid and alkaline solution. *ACS Sustain. Chem. Eng.* 6, 15162–15169. doi:10.1021/acsschemeng.8b03638
- Goberna-Ferrón, S., Soriano-López, J., and Galán-Mascarós, J. R. (2015). Activity and stability of the tetramanganese polyanion [Mn₄(H₂O)₂(PW₉O₃₄)₂]¹⁰⁻ during electrocatalytic water oxidation. *Inorganics* 3, 332–340. doi:10.3390/inorganics3030332
- Guan, J., Liu, Y., Fang, Y., Du, X., Fu, Y., Wang, L., et al. (2021). Co-Ni alloy nanoparticles supported by carbon nanofibers for hydrogen evolution reaction. *J. Alloys Compd.* 868, 159172. doi:10.1016/j.jallcom.2021.159172
- Gusmão, F. M. B., Mladenović, D., Radinović, K., Santos, D. M. F., and Šljukić, B. (2022). Polyoxometalates as electrocatalysts for electrochemical energy conversion and storage. *Energies* 15, 9021. doi:10.3390/en15239021
- Horn, M. R., Singh, A., Alomari, S., Goberna-Ferrón, S., Benages-Vilau, R., Chodankar, N., et al. (2021). Polyoxometalates (POMs): from electroactive clusters to energy materials. *Energy Environ. Sci.* 14, 1652–1700. doi:10.1039/D0EE03407J
- Huang, H., Shen, B., Yan, M., He, H., Yang, L., Jiang, Q., et al. (2022). Coupled spinel manganese-cobalt oxide and MXene electrocatalysts towards efficient hydrogen evolution reaction. *Fuel* 328, 125234. doi:10.1016/j.fuel.2022.125234
- Imani, A. H., Ojani, R., and Raouf, J. B. (2018). *In situ* synthesis of a novel organic-inorganic composite as a non-noble metal electrocatalyst for the oxygen evolution reaction. *Int. J. Hydrogen Energy* 43, 8267–8277. doi:10.1016/j.ijhydene.2018.03.032
- Imani, A. H., Ojani, R., and Raouf, J. B. (2021). Novel polyoxometalate-based composite as efficient electrocatalyst for alkaline water oxidation reaction. *J. Iran. Chem. Soc.* 18, 2079–2089. doi:10.1007/s13738-021-02169-0
- Intergovernmental Panel for Climate Change (IPCC) (2018). “Summary for policymakers,” in: *global Warming of 1.5°C. An IPCC Special Report on the impacts of global warming of 1.5°C above pre-industrial levels and related global greenhouse gas emission pathways in the context of strengthening the global response to the threat of climate change, sustainable development and efforts to eradicate poverty*, 3–24. doi:10.1017/9781009157940.001
- Jawale, D. V., Fossard, F., Miserque, F., Geertsen, V., Teillout, A.-L., de Oliveira, P., et al. (2022). Carbon nanotube-polyoxometalate nanohybrids as efficient electrocatalysts for the hydrogen evolution reaction. *Carbon* 188, 523–532. doi:10.1016/j.carbon.2021.11.046
- Jeong, S., Hu, K., Ohto, T., Nagata, Y., Masuda, H., Fujita, J., et al. (2020). Effect of graphene encapsulation of NiMo alloys on oxygen evolution reaction. *ACS Catal.* 10, 792–799. doi:10.1021/acscatal.9b04134
- Ji, S.-M., Muthurasu, A., and Kim, H. Y. (2023). Marigold flower-shaped metal-organic framework supported manganese vanadium oxide electrocatalyst for efficient oxygen evolution reactions in an alkaline medium. *Chem. Eur. J.* 29, e202300137. doi:10.1002/chem.202300137
- Jia, X., Streb, C., and Song, Y.-F. (2019). Devisable POM/Ni foam composite: precisely control synthesis toward enhanced hydrogen evolution reaction at high pH. *Chem. Eur. J.* 25, 15548–15554. doi:10.1002/chem.201903059
- Jia, Y., Xue, Z., Li, Y., and Li, G. (2022). Recent progress of metal organic frameworks-based electrocatalysts for hydrogen evolution, oxygen evolution, and oxygen reduction reaction. *Energy Environ. Mat.* 5, 1084–1102. doi:10.1002/eeem.12290
- Jiang, B., Wang, T., Cheng, Y., Liao, F., Wu, K., and Shao, M. (2018). Ir/g-C₃N₄/Nitrogen-Doped graphene nanocomposites as bifunctional electrocatalysts for overall water splitting in acidic electrolytes. *ACS Appl. Mat. Interfaces* 10, 39161–39167. doi:10.1021/acscami.8b11970
- Jiang, J., Zhang, C., and Ai, L. (2016). Hierarchical iron nickel oxide architectures derived from metal-organic frameworks as efficient electrocatalysts for oxygen evolution reaction. *Electrochim. Acta* 208, 17–24. doi:10.1016/j.electacta.2016.05.008
- Jiang, S., Duan, C., Li, X., Wand, D., Wang, Z., Sun, H., et al. (2021). Alloying strategy for constructing multi-component nano-catalysts towards efficient and durable oxygen evolution in alkaline electrolyte. *Electrochim. Acta* 391, 138933. doi:10.1016/j.electacta.2021.138933
- Kang, Q., Lai, D., Su, M., Xiong, B., Tang, W., Lu, Q., et al. (2022). Tailored dodecahedral polyoxometalates nanoframes with *in situ* encapsulated Co, Ni, C for oxygen evolution reaction. *Chem. Eng. J.* 430, 110116. doi:10.1016/j.cej.2021.133116
- Katsunaros, I., Cherevko, S., Zeradjanin, A. R., and Mayrhofer, K. J. J. (2014). Oxygen electrochemistry as a cornerstone for sustainable energy conversion. *Angew. Chem. Int. Ed.* 53, 102–121. doi:10.1002/anie.201306588
- Katubi, K. M., Warsi, A.-Z., Aziz, F., Khattak, Z., Warsi, M. F., Al-buriah, M. S., et al. (2023). Tungsten oxide-copper oxide supported on reduced graphene oxide as a proficient electrocatalyst with enhanced hydrogen evolution efficiency in an alkaline media. *Curr. Appl. Phys.* 51, 80–90. doi:10.1016/j.cap.2023.05.002
- Kim, A., Muthuhamy, N., Yoon, C., Joo, S. H., and Park, K. H. (2018). MOF-derived Cu₂O nanocatalyst for oxygen reduction reaction and cycloaddition reaction. *Nanomaterials*, 8. doi:10.3390/nano8030138
- Kumar, M., Jeong, D. I., and Yoon, D. H. (2020). Copper nickel alloy nanorods textured nanoparticles for oxygen evolution reaction. *Electrochim. Acta* 333, 135545. doi:10.1016/j.electacta.2019.135545
- Lee, J.-W., and Popov, B. N. (2007). Ruthenium-based electrocatalysts for oxygen reduction reaction—a review. *J. Solid State Electrochem.* 11, 1355–1364. doi:10.1007/s10008-007-0307-3
- Li, G., Zhang, X., Zhang, H., Liao, C., and Jiang, G. (2019). Bottom-up MOF-intermediated synthesis of 3D hierarchical flowerlike cobalt-based homobimetallic eficiente composed of ultrathin nanosheets for highly efficient oxygen evolution reaction. *Appl. Catal. B-Environ.* 15, 147–154. doi:10.1016/j.apcatb.2019.03.007

- Li, H., Liu, Y., He, F., Yang, H., Li, Z., Zhou, Q., et al. (2020). *In situ* grown Cu-Based metal-organic framework on copper foam as high-performance electrocatalysts for oxygen evolution reaction. *Int. J. Hydrogen Energy* 45, 21540–21546. doi:10.1016/j.ijhydene.2020.05.234
- Lim, D., Oh, E., Lim, C., Shim, S. E., and Baeck, S.-H. (2020). Bimetallic NiFe alloys as highly efficient electrocatalysts for the oxygen evolution reaction. *Catal. Today* 352, 27–33. doi:10.1016/j.cattod.2019.09.046
- Limani, N., Marques, I. S., Jarrais, B., Fernandes, A. J. S., Freire, C., and Fernandes, D. M. (2022). Cobalt phosphotungstate-based composites as bifunctional electrocatalysts for oxygen reactions. *Catalysts* 12, 357. doi:10.3390/catal12040357
- Liu, K., Zhang, C., Sun, Y., Zhang, G., Shen, X., Zou, F., et al. (2018). High-performance transition metal phosphide alloy catalyst for oxygen evolution reaction. *ACS Nano* 12, 158–167. doi:10.1021/acsnano.7b04646
- Liu, R., Cao, K., Clark, A. H., Lu, P., Anjass, M., Biskupek, J., et al. (2020). Top-down synthesis of polyoxometalate-like subnanometer molybdenum-oxo clusters as high-performance electrocatalysts. *Chem. Sci.* 11, 1043–1051. doi:10.1039/C9SC05469C
- Liu, S.-W., and Qin, X. (2015). Manganese oxides/graphene composite as cathode catalyst for the oxygen reduction reaction in alkaline solution. *Fullerenes, Nanotub. Carbon Nanostructures* 23, 824–830. doi:10.1080/1536383X.2015.1009533
- Liu, T., Li, P., Yao, N., Cheng, G., Chen, S., Luo, W., et al. (2019). CoP-doped MOF-based electrocatalyst for pH-universal hydrogen evolution reaction. *Angew. Chem. Int. Ed.* 58, 4679–4684. doi:10.1002/anie.201901409
- Liu, X., Niu, J., Rajendran, S., Lei, Y., Qin, J., and Zhang, X. (2021). Electrodeposition of the manganese-doped nickelphosphorus catalyst with enhanced hydrogen evolution reaction activity and durability. *Int. J. Hydrogen Energy* 47, 41994–42000. doi:10.1016/j.ijhydene.2021.10.105
- Lu, H.-S., Zhang, H., Liu, R., Zhang, X., Zhao, H., and Wang, G. (2017). Macroscale cobalt-MOFs derived metallic Co nanoparticles embedded in N-doped porous carbon layers as efficient oxygen electrocatalysts. *Appl. Surf. Sci.* 392, 402–409. doi:10.1016/j.apusc.2016.09.045
- Lu, X. F., Xia, B. Y., Zang, S.-Q., and Lou, X. W. (2019). Metal-organic frameworks based electrocatalysts for the oxygen reduction reaction. *Angew. Chem. Int. Ed.* 59, 4634–4650. doi:10.1002/anie.201910309
- Luo, W., Hu, J., Diao, H., Schwarz, B., Streb, C., and Song, Y.-F. (2017a). Robust polyoxometalate/nickel foam composite electrodes for sustained electrochemical oxygen evolution at high pH. *Angew. Chem. Int. Ed.* 56, 4941–4944. doi:10.1002/anie.201612232
- Luo, X.-F., Wang, J., Liang, Z.-S., Chen, S.-Z., Liu, Z.-L., Xu, C.-W., et al. (2017b). Manganese oxide with different morphology as efficient electrocatalyst for oxygen evolution reaction. *Int. J. Hydrogen Energy* 42, 7151–7157. doi:10.1016/j.ijhydene.2016.04.162
- Ma, X., Qi, K., Wei, S., Zhang, L., and Cui, X. (2019). *In situ* encapsulated nickel-copper nanoparticles in metal-organic frameworks for oxygen evolution reaction. *J. Alloys Compd.* 770, 236–242. doi:10.1016/j.jallcom.2018.08.096
- Mani, P., Devadas, S., Gurusamy, T., Karthik, P. E., Ratheesh, B. P., Ramanujam, K., et al. (2019). Sodalite-type Cu-based three-dimensional metal-organic framework for efficient oxygen reduction reaction. *Chem. Asian J.* 14, 4814–4818. doi:10.1002/asia.201901242
- Marques, I. S., Jarrais, B., Mbomekallé, I.-M., Teillout, A. - L., de Oliveira, P., Freire, C., et al. (2022). Synergetic effects of mixed-metal Polyoxometalates@Carbon-based composites as electrocatalysts for the oxygen reduction and the oxygen evolution reactions. *Catalysts* 12, 440. doi:10.3390/catal12040440
- Mladenović, D., Daş, E., Santos, D. M. F., Yurtcan, A. B., Miljanić, Š., and Šljukić, B. (2022). Boosting oxygen electrode kinetics by addition of cost-effective transition metals (Ni, Fe, Cu) to platinum on graphene nanoplatelets. *J. Alloys Compd.* 905, 164156. doi:10.1016/j.jallcom.2022.164156
- Mladenović, D., Daş, E., Santos, D. M. F., Yurtcan, A. B., and Šljukić, B. (2023b). Highly efficient oxygen electrode obtained by sequential deposition of transition metal-platinum alloys on graphene nanoplatelets. *Materials* 16, 3388. doi:10.3390/ma16093388
- Mladenović, D., Mladenović, A., Santos, D. M. F., Yurtcan, A. B., Miljanić, Š., Mentus, S., et al. (2023a). Transition metal oxides for bifunctional ORR/OER electrocatalysis in unitized regenerative fuel cells. *J. Electroanal. Chem.* 946, 117709. doi:10.1016/j.jelechem.2023.117709
- Mladenović, D., Santos, D. M. F., Bozkurt, G., Soyulu, G. S. P., Yurtcan, A. B., Miljanić, Š., et al. (2021). Tailoring metal-oxide-supported PtNi as bifunctional catalysts of superior activity and stability for unitised regenerative fuel cell applications. *Electrochem. Commun.* 124, 106963. doi:10.1016/j.elecom.2021.106963
- Moschkowitsch, W., Zion, N., Honig, H. C., Levy, N., Cullen, D. A., and Elbaz, L. (2022). Mixed-metal Nickel-Iron oxide aerogels for oxygen evolution reaction. *ACS Catal.* 12, 12162–12169. doi:10.1021/acscatal.2c03351
- Mukherjee, A., Chakraborty, S., Su, W.-N., and Basu, S. (2018). Nanostructured nickel ferrite embedded in reduced graphene oxide for electrocatalytic hydrogen evolution reaction. *Mat. Today Energy* 8, 118–124. doi:10.1016/j.mtener.2018.03.004
- Muralikrishna, S., Ravishankar, T. N., Ramakrishnapa, T., Nagaraju, D. H., and Pai, R. K. (2015). Non-noble metal graphene oxide-copper (II) ions hybrid electrodes for electrocatalytic hydrogen evolution reaction. *Environ. Prog. Sustain. Energy* 35, 565–573. doi:10.1002/ep.12238
- Nakagawa, T., Bjorge, N. S., and Murray, R. W. (2009). Electrogenerated IrO_x nanoparticles as dissolved redox catalysts for water oxidation. *J. Am. Chem. Soc.* 131, 15578–15579. doi:10.1021/ja9063298
- Nivetha, R., Sajeev, A., Paul, A. M., Gothandapani, K., Gnanasekar, S., Bhardwaj, P., et al. (2020). Cu based Metal Organic Framework (Cu-MOF) for electrocatalytic hydrogen evolution reaction. *Mat. Res. Express* 7, 114001. doi:10.1088/2053-1591/abb056
- Pan, Z., Pan, N., Chen, L., He, J., and Zhang, M. (2019). Flower-like MOF-derived Co-N-doped carbon composite with remarkable activity and durability for electrochemical hydrogen evolution reaction. *Int. J. Hydrogen Energy* 44, 30075–30083. doi:10.1016/j.ijhydene.2019.09.117
- Park, Y. S., Park, C. S., Kim, C. H., Kim, Y. D., Park, S., and Lee, J. H. (2016). Characteristics of the oxygen evolution reaction on synthetic copper – cobalt – oxide electrodes for water electrolysis. *J. Korean Phys. Soc.* 69, 1187–1190. doi:10.3938/jkps.69.1187
- Peng, K., Bhuvanendran, N., Ravichandran, S., Xu, Z., Zhang, W., Ma, Q., et al. (2020). Sewage sludge-derived Fe- and N-containing porous carbon as efficient support for Pt catalyst with superior activity towards methanol electrooxidation. *Int. J. Hydrogen Energy* 45, 9795–9802. doi:10.1016/j.ijhydene.2020.01.140
- Pratama, D. S. A., Haryanto, A., and Lee, C. W. (2023). Heterostructured mixed metal oxide electrocatalyst for the hydrogen evolution reaction. *Front. Chem.* 11, 1141361. doi:10.3389/fchem.2023.1141361
- Qin, X., Huang, Y., Wang, K., Xu, T., Wang, Y., Wang, M., et al. (2019). Highly efficient oxygen reduction reaction catalyst derived from Fe/Ni mixed-Metal-Organic frameworks for application of fuel cell cathode. *Ind. Eng. Chem. Res.* 58, 10224–10237. doi:10.1021/acs.iecr.9b01412
- Rehman, I. u., Zhang, J., Chen, J., and Wang, R. (2022). *In situ* derived Ni-N-CNTs from ZIF-8 crystals as efficient electrocatalysts for oxygen reduction reaction. *Inorg. Chem. Commun.* 144, 109922. doi:10.1016/j.inoche.2022.109922
- Ritchie, H., Roser, M., and Rosado, P. (2022). Energy published online at OurWorldInData.org. Available at: <https://ourworldindata.org/energy>.
- Rousseau, G., Zhang, S., Oms, O., Dolbecq, A., Marrot, J., Liu, R., et al. (2015). Sequential synthesis of 3 d–3d, 3 d–4d, and 3 d–5d hybrid polyoxometalates and application to the electrocatalytic oxygen reduction reactions. *Chemistry* 21, 12153–12160. doi:10.1002/chem.201501609
- Roy, A., Jadhav, H. S., Cho, M., and Seo, J. G. (2019). Electrochemical deposition of self-supported bifunctional copper oxide anchored mesoporous fullerene nanohybrids and oxygen evolution reaction. *J. Ind. Eng. Chem.* 76, 515–523. doi:10.1016/j.jiec.2019.04.019
- Saianand, G., Gopalan, A.-L., Lee, J.-C., Sathish, C., Gopalakrishnan, K., Unni, G. E., et al. (2020). Mixed copper/copper-oxide anchored mesoporous fullerene nanohybrids as superior electrocatalysts toward oxygen reduction reaction. *Small* 16, e1903937. doi:10.1002/sml.201903937
- Sajeev, A., Sathyaseelan, A., Bejigo, K. S., and Kim, S. J. (2023). Trimetallic non-noble NiCoSn alloy as an efficient electrocatalyst towards methanol oxidation and oxygen reduction reactions. *J. Colloid Interface Sci.* 637, 363–371. doi:10.1016/j.jcis.2023.01.064
- Sanji, F. D., Balakrishnan, P., Su, H., Khotseng, L., and Xu, Q. (2021). Fabrication of polyoxometalate-modified palladium-nickel/reduced graphene oxide alloy catalysts for enhanced oxygen reduction reaction activity. *RSC Adv.* 11, 39118–39129. doi:10.1039/D1RA06936E
- Shen, Q., Zhang, C., Wang, M., Pang, H., Ma, H., Wang, X., et al. (2019). A novel Lindqvist intercalation compound: synthesis, crystal structure and hydrogen evolution reaction performance. *Inorg. Chem. Commun.* 99, 64–69. doi:10.1016/j.inoche.2018.11.013
- Shen, Y., Zhou, Y., Wang, D., Wu, X., Li, J., and Xi, J. (2017). Nickel-copper alloy encapsulated in graphitic carbon shells as electrocatalysts for hydrogen evolution reaction. *Adv. Energy Mat.* 8. doi:10.1002/aenm.201701759
- Sidhureddy, B., Prins, S., Wen, J., Thirupathi, A. R., Govindhan, M., and Chen, A. (2019). Synthesis and electrochemical study of mesoporous nickel-cobalt oxides for efficient oxygen reduction. *ACS Appl. Mat. Interfaces* 11, 18295–18304. doi:10.1021/acsami.8b22351
- Sivakumar, P., Subramanian, P., Maiyalagan, T., Gedanken, A., and Schecter, A. (2019). Ternary nickel cobalt manganese spinel oxide nanoparticles as heterogeneous electrocatalysts for oxygen evolution and oxygen reduction reaction. *Mater. Chem. Phys.* 229, 190–196. doi:10.1016/j.matchemphys.2019.03.017
- Song, Y., Peng, Y., Yao, S., Zhang, P., Wang, Y., Gu, J., et al. (2022). Co-POM@MOF-derivatives with trace cobalt content for highly efficient oxygen reduction. *Chin. Chem. Lett.* 33, 1047–1050. doi:10.1016/j.ccl.2021.08.045
- Sood, P., Joshi, A., and Singh, M. (2022). A rare polyoxometalate cluster [NiW₁₂O₄₄]¹⁴⁻ based solid as a pre-catalyst for efficient and long-term oxygen evolution. *Nanoscale Adv.* 4, 5015–5020. doi:10.1039/D2NA00646D
- Sun, B., Wang, S., Li, X., Zhang, W., Li, J., Pan, Q., et al. (2023). Giant polyoxomolybdate clusters -derived bimetallic Ni/Mo₂C catalyst for electrochemical

- hydrogen evolution. *Int. J. Hydrogen Energy* 48, 9353–9361. doi:10.1016/j.ijhydene.2022.12.101
- Sun, R.-M., Yao, Y.-Q., Wang, A.-J., Fang, K.-M., Zhang, L., and Feng, J.-J. (2021). One-step pyrolysis synthesis of nitrogen, manganese-codoped porous carbon encapsulated cobalt-iron nanoparticles with superior catalytic activity for oxygen reduction reaction. *J. Colloid Interface Sci.* 592, 405–415. doi:10.1016/j.jcis.2021.02.071
- Sun, T., Wu, Q., Che, R., Bu, Y., Jiang, Y., Li, Y., et al. (2015). Alloyed Co–Mo nitride as high-performance electrocatalyst for oxygen reduction in acidic medium. *ACS Catal.* 5, 1857–1862. doi:10.1021/cs502029h
- Swetha, J. V., Parse, H., Kakade, B., and Geetha, A. (2018). Morphology dependent facile synthesis of manganese oxide nanostructures for oxygen reduction reaction. *Solid State Ion.* 328, 1–7. doi:10.1016/j.ssi.2018.11.002
- Tahir, M., Pan, L., Idrees, F., Zhang, X., Wang, L., Zou, J.-J., et al. (2017). Electrocatalytic oxygen evolution reaction for energy conversion and storage: a comprehensive review. *Nano Energy* 37, 136–157. doi:10.1016/j.nanoen.2017.05.022
- Tong, Y., Liang, Y., Hu, Y., Shamsaei, E., Wei, J., Hao, Y., et al. (2020). Synthesis of ZIF/CNT nanonecklaces and their derived cobalt nanoparticles/N-doped carbon catalysts for oxygen reduction reaction. *J. Alloys Compd.* 816, 152684. doi:10.1016/j.jallcom.2019.152684
- Tseng, C.-Y., Cheng, I.-C., and Chen, J.-Z. (2022). Low-pressure-plasma-processed NiFe-MOFs/nickel foam as an efficient electrocatalyst for oxygen evolution reaction. *Int. J. Hydrogen Energy* 47, 35990–35998. doi:10.1016/j.ijhydene.2022.08.179
- Vij, V., Sultan, S., Harzandi, A. M., Meena, A., Tiwari, J. N., Lee, W.-G., et al. (2017). Nickel-based electrocatalysts for energy-related applications: oxygen reduction, oxygen Evolution, and hydrogen evolution reactions. *ACS Catal.* 7, 7196–7225. doi:10.1021/acscatal.7b01800
- Wahab, A., Iqbal, N., Noor, T., Ashraf, S., Raza, M. A., Ahmad, A., et al. (2020). Thermally reduced mesoporous manganese MOF @reduced graphene oxide nanocomposite as bifunctional electrocatalyst for oxygen reduction and evolution. *RSC Adv.* 10, 27728–27742. doi:10.1039/D0RA04193A
- Wang, C., Song, Y., Cong, W., Yan, Y., Wang, M., and Zhou, J. (2023). From surface loading to precise confinement of polyoxometalates for electrochemical energy storage. *Chin. Chem. Lett.* 34, 108194. doi:10.1016/j.ccl.2023.108194
- Wang, C., Yang, H., Zhang, Y., and Wang, Q. (2019). NiFe alloy nanoparticles with hcp crystal structure stimulate superior oxygen evolution reaction electrocatalytic activity. *Angew. Chem. Int. Ed.* 58, 6099–6103. doi:10.1002/anie.201902446
- Wang, H., Ma, N., Cao, Y., Yu, H., Zuo, J., Fan, W., et al. (2019). Cobalt and cobalt oxide supported on nitrogen-doped porous carbon as electrode materials for hydrogen evolution reaction. *Int. J. Hydrogen Energy* 44, 3649–3657. doi:10.1016/j.ijhydene.2018.12.107
- Wang, L., Wang, A., Xue, Z.-Z., Hu, J.-X., Han, S.-D., and Wang, G.-M. (2022). Ultrathin two-dimensional polyoxometalate-based Metal–Organic framework nanosheets for efficient electrocatalytic hydrogen evolution. *Inorg. Chem.* 61, 18311–18317. doi:10.1021/acs.inorgchem.2c03431
- Wang, X., Hou, X., Lee, H., Lu, L., Wu, X., Sun, L., et al. (2020). Copper selenide-derived copper oxide nanoplates as a durable and efficient electrocatalyst for oxygen evolution reaction. *Energy Technol.* 8. doi:10.1002/ente.202000142
- Wang, Z., Li, M., Fan, L., Han, J., and Xiong, Y. (2017). Fe/Ni-N-CNFs electrochemical catalyst for oxygen reduction reaction/oxygen evolution reaction in alkaline media. *Appl. Surf. Sci.* 401, 89–99. doi:10.1016/j.apsusc.2016.12.242
- Wu, L.-Z., Zhou, X.-Y., Zeng, P.-C., Huang, J.-Y., Zhang, M.-D., and Qin, L. (2022). Hydrothermal synthesis of Ni(II) or Co(II)-based MOF for electrocatalytic hydrogen evolution. *Polyhedron* 225, 116035. doi:10.1016/j.poly.2022.116035
- Wu, Y., Sun, R., and Cen, J. (2020). Facile synthesis of cobalt oxide as an efficient electrocatalyst for hydrogen evolution reaction. *Front. Chem.* 8, 386. doi:10.3389/fchem.2020.00386
- Wu, Z., Vagin, M., Boyd, R., Ding, P., Pshyk, O., Greczynski, G., et al. (2023). Selectivity control of oxygen reduction reaction over mesoporous transition metal oxide catalysts for electrified purification technologies. *ACS Appl. Mat. Interfaces* 15, 26093–26103. doi:10.1021/acscami.3c01196
- Wu, Z.-P., Lu, X. F., Zang, S.-Q., and Lou, X. W. (2020). Non-noble-metal-based electrocatalysts toward the oxygen evolution reaction. *Adv. Funct. Mat.* 30. doi:10.1002/adfm.201910274
- Xing, X., Liu, R., Cao, K., Kaiser, U., Zhang, G., and Streb, C. (2018). Manganese vanadium Oxide–N-doped reduced graphene oxide composites as oxygen reduction and oxygen evolution electrocatalysts. *ACS Appl. Mat. Interfaces* 10, 44511–44517. doi:10.1021/acscami.8b16578
- Xu, C., Li, J., Sun, D., Li, X., Wang, X., and Su, Z. (2021). Co/WC@NC electrocatalysts derived from polyoxometalates (POM) for efficient hydrogen evolution. *Nanotechnology* 32. doi:10.1088/1361-6528/ac084d
- Xu, H., Li, F., Li, Z., Liu, Q., Li, B., Xu, L., et al. (2022). Research progress of metal oxide as cathode materials for hydrogen evolution. *Int. J. Electrochem. Sci.* 17, 221249. doi:10.20964/2022.12.49
- Xu, S., Lv, C., He, T., Huang, Z., and Zhang, C. (2019). Amorphous film of cerium doped cobalt oxide as a highly efficient electrocatalyst for oxygen evolution reaction. *J. Mat. Chem. A* 7, 7526–7532. doi:10.1039/C9TA00061E
- Xu, Y., Zhang, X., Liu, Y., Wang, R., Yang, Y., and Chen, J. (2023). A critical review of research progress for metal alloy materials in hydrogen evolution and oxygen evolution reaction. *Environ. Sci. Pollut. Res.* 30, 11302–11320. doi:10.1007/s11356-022-24728-5
- Yan, Z., Liu, H., Hao, Z., Yu, M., Chen, X., and Chen, J. (2020). Electrodeposition of (hydro)oxides for an oxygen evolution electrode. *Chem. Sci.* 11, 10614–10625. doi:10.1039/D0SC01532F
- Ye, C., Wang, Z., and Shen, Y. (2022). Preparation of iron-copper oxalates and oxides for the oxygen evolution reaction. *J. Electrochem. Soc.* 169, 064503. doi:10.1149/1945-7111/ac7259
- Yu, L., Lin, J., Zheng, M., Chen, M., and Ding, Y. (2018). Homogeneous electrocatalytic water oxidation at neutral pH by a robust trinuclear copper(II)-substituted polyoxometalate. *Chem. Commun.* 54, 354–357. doi:10.1039/C7CC08301G
- Yusibova, G., Assafrei, J.-M., Ping, K., Aruväli, J., Paiste, P., Käärik, M., et al. (2023). Bimetallic metal-organic-framework-derived porous cobalt manganese oxide bifunctional oxygen electrocatalyst. *J. Electroanal. Chem.* 930, 117161. doi:10.1016/j.jelechem.2023.117161
- Zand, Z., Mohammadi, M. R., Sologubenko, A. S., Handschin, S., Bagheri, R., Chernev, P., et al. (2023). Oxygen evolution reaction by silicate-stabilized manganese oxide. *ACS Appl. Energy Mat.* 6, 1702–1713. doi:10.1021/acsaem.2c03587
- Zang, D., Huang, Y., Li, Q., Tang, Y., and Wei, Y. (2019). Cu dendrites induced by the Anderson-type polyoxometalate NiMo6O24 as a promising electrocatalyst for enhanced hydrogen evolution. *Appl. Catal. B-Environ* 249, 163–171. doi:10.1016/j.apcatb.2019.02.039
- Zeb, Z., Huang, Y., Chen, L., Zhou, W., Liao, M., Jiang, Y., et al. (2023). Comprehensive overview of polyoxometalates for electrocatalytic hydrogen evolution reaction. *Coord. Chem. Rev.* 482, 215058. doi:10.1016/j.ccr.2023.215058
- Zeng, J., Chen, L., Li, L., Yang, W., Zou, H., and Chen, S. (2020). Effect of PEG on performance of NiMnO catalyst for hydrogen evolution reaction. *Front. Chem.* 8, 281. doi:10.3389/fchem.2020.00281
- Zhai, H., Gao, T., Qi, T., Zhang, Y., Zeng, G., and Xiao, D. (2017). Iron–cobalt phosphomolybdate with high electrocatalytic activity for oxygen evolution reaction. *Chem. Asian J.* 12, 2694–2702. doi:10.1002/asia.201700905
- Zhang, C., Hwang, S. Y., Trout, A., and Peng, Z. (2014). Solid-state chemistry-enabled scalable production of octahedral Pt–Ni alloy electrocatalyst for oxygen reduction reaction. *J. Am. Chem. Soc.* 136, 7805–7808. doi:10.1021/ja501293x
- Zhang, C., Shen, X., Pan, Y., and Peng, Z. (2017). A review of Pt-based electrocatalysts for oxygen reduction reaction. *Front. Energy* 11, 268–285. doi:10.1007/s11708-017-0466-6
- Zhang, L., Chen, S., Dai, Y., Shen, Z., Wei, M., Huang, R., et al. (2018). Copper–Palladium tetrapods with sharp tips as a superior catalyst for the oxygen reduction reaction. *ChemCatChem* 10, 925–930. doi:10.1002/cctc.201701578
- Zhang, L., Pang, D., Cao, X., Ma, Y., Kou, Y., Liu, Z., et al. (2022a). Phosphorus modified hollow, porous Nickel–Cobalt oxides nanocubes with heterostructure for oxygen evolution reaction in alkaline. *J. Alloys Compd.* 925, 166338. doi:10.1016/j.jallcom.2022.166338
- Zhang, M., Hu, D., Xu, Z., Liu, B., Boubeche, M., Chen, Z., et al. (2021). Facile synthesis of Ni–Co–Cu-metal organic frameworks electrocatalyst boosting for hydrogen evolution reaction. *J. Mat. Sci. Technol.* 72, 172–179. doi:10.1016/j.jmst.2020.09.028
- Zhang, M.-c., Liu, M.-y., Yang, M.-x., Liu, X.-x., Shen, S.-y., Wu, J.-s., et al. (2023c). Copper–cobalt bimetallic conductive metal–organic frameworks as bifunctional oxygen electrocatalyst in alkaline and neutral media. *J. Solid State Chem.* 325, 124133. doi:10.1016/j.jssc.2023.124133
- Zhang, Q., Wei, Z. D., Liu, C., Liu, X., Qi, X. Q., Chen, S. G., et al. (2012). Copper-doped cobalt oxide electrodes for oxygen evolution reaction prepared by magnetron sputtering. *Int. J. Hydrogen Energy* 37, 822–830. doi:10.1016/j.ijhydene.2011.04.051
- Zhang, S., Oms, O., Hao, L., Liu, R., Wang, M., Zhang, Y., et al. (2017). High oxygen reduction reaction performances of cathode materials combining polyoxometalates, coordination complexes, and carbonaceous supports. *ACS Appl. Mat. Interfaces* 9, 38486–38498. doi:10.1021/acscami.7b10989
- Zhang, X., Ding, K., Weng, B., Liu, S., Jin, W., Ji, X., et al. (2020). Coral-like carbon-wrapped NiCo alloys derived by emulsion aggregation strategy for efficient oxygen evolution reaction. *J. Colloid Interface Sci.* 573, 96–104. doi:10.1016/j.jcis.2020.03.124
- Zhang, X., Li, Y., Guo, Y., Hu, A., Li, M., Hang, T., et al. (2019). 3D hierarchical nanostructured Ni–Co alloy electrodes on porous nickel for hydrogen evolution reaction. *Int. J. Hydrogen Energy* 44, 29946–29955. doi:10.1016/j.ijhydene.2019.09.193
- Zhang, Z., Enze, F., Shuangqi, Z., Zhaojun, W., Wenzhi, Z., Ming, Z., et al. (2023a). A new two-fold interpenetrating metal-organic framework based on polyoxometalate: synthesis, structure, efficient hydrogen evolution and dye degradation. *J. Solid State Chem.* 323, 124066. doi:10.1016/j.jssc.2023.124066

- Zhang, Z., Ran, J., Fan, E., Zhou, S., Chai, D.-F., Zhang, W., et al. (2023b). Mesoporous CoMoO_4 hollow tubes derived from POMOFs as efficient electrocatalyst for overall water splitting. *J. Alloys Compd.* 968, 172169. doi:10.1016/j.jallcom.2023.172169
- Zhang, Z., Ran, J., Wu, Z., and Zhao, B. (2022). Hierarchical Ni modified PW_{12} clusters *in situ* integrated on Ni foam for efficient alkaline hydrogen evolution. *J. Clust. Sci.* 34, 1475–1482. doi:10.1007/s10876-022-02318-2
- Zhao, L., Gong, C., Chen, X., He, X., Chen, H., Du, X., et al. (2023). ZIF-67 derived Mo-CoS_2 nanoparticles embedded in hierarchically porous carbon hollow sphere for efficient overall water splitting in. *Appl. Surf. Sci.* 623, 16184. doi:10.1016/j.apsusc.2023.157030
- Zhao, S., Wang, Y., Dong, J., He, C.-T., Yin, H., An, P., et al. (2016). Ultrathin metal-organic framework nanosheets for electrocatalytic oxygen evolution. *Nat. Energy* 1, 16184–16210. doi:10.1038/nenergy.2016.184
- Zhao, S., Zhao, X., Zhang, H., Li, J., and Zhu, Y. (2017). Covalent combination of polyoxometalate and graphitic carbon nitride for light-driven hydrogen peroxide production. *Nano Energy* 35, 405–414. doi:10.1016/j.nanoen.2017.04.017
- Zhao, X., Pachfule, P., Li, S., Simke, J. R. J., Schimdt, J., and Arne, T. (2018). Bifunctional electrocatalysts for overall water splitting from an iron/nickel-based bimetallic metal-organic framework/dicyandiamide composite. *Angew. Chem. Int. Ed.* 57, 9059–9064. doi:10.1002/ange.201803136
- Zheng, Y., Xu, X., Chen, J., and Wang, Q. (2021). Surface O_2 -regulation on POM electrocatalyst to achieve accurate $2e^-/4e^-$ ORR control for H_2O_2 production and Zn-air battery assemble. *Appl. Catal. B-Environ.* 285, 119788. doi:10.1016/j.apcatb.2020.119788
- Zhou, W., Huang, D.-D., Wu, Y.-P., Zhao, J., Wu, T., Zhang, J., et al. (2019). Stable hierarchical bimetal-organic nanostructures as high performance electrocatalysts for the oxygen evolution reaction. *Angew. Chem. Int. Ed.* 58, 4227–4231. doi:10.1002/anie.201813634
- Zhou, W., Xue, Z., Liu, Q., Li, Y., Hu, J., and Li, G. (2020). Trimetallic MOF-74 films grown on Ni foam as bifunctional electrocatalysts for overall water splitting. *ChemSusChem* 13, 5647–5653. doi:10.1002/cssc.202001230
- Zhu, X., Shi, X., Asiri, A. M., Luo, Y., and Sun, X. (2018). Efficient oxygen evolution electrocatalyzed by a Cu nanoparticle-embedded N-doped carbon nanowire array. *Inorg. Chem. Front.* 5, 1188–1192. doi:10.1039/C8SQI00119G